- 1 Formation and evolution of aqSOA from aqueous-phase reactions
- 2 of phenolic carbonyls: comparison between ammonium sulfate
- 3 and ammonium nitrate solutions
- 5 Dan Dan Huang<sup>1,§</sup>, Qi Zhang<sup>2,\*</sup>, Heidi H.Y. Cheung<sup>3</sup>, Lu Yu<sup>2,#</sup>, Shan Zhou<sup>2,†</sup>, Cort Anastasio<sup>4</sup>,
- 6 Jeremy D. Smith<sup>4,††</sup>, Chak K. Chan<sup>l,\*</sup>

4

- 8 <sup>1</sup> School of Energy and Environment, City University of Hong Kong, Hong Kong, China
- 9 <sup>2</sup> Department of Environmental Toxicology, University of California, 1 Shields Ave. Davis,
- 10 CA 95616, USA
- <sup>3</sup> Division of Environment, Hong Kong of University of Science and Technology, Hong
- 12 Kong, China
- <sup>4</sup> Department of Land, Air and Water Resources, University of California, 1 Shields Ave,
- 14 Davis, CA 95616, USA

15

- 16 \*Corresponding authors:
- 17 Qi Zhang, dkwzhang@ucdavis.edu; Phone: 530-752-5779 (Office); Fax: 530-752-3394
- 18 Chak K. Chan, <u>Chak.K.Chan@cityu.edu.hk</u>; Phone: 852 3442-5593; Fax: 852-3442-0688
- 19 § Currently at Shang Hai Academy of Environmental Sciences, Shang Hai, China
- 20 \*\*Currently at BOE technologies, Inc., USA
- <sup>†</sup> Currently at Syracuse University, NY, USA
- 22 <sup>††</sup> Currently at California Air Resources Board, CA, USA

23

#### **Abstract:**

25

26

27

28

29

30

31

32

33

34

35

36

37

38

39

40

41

42

43

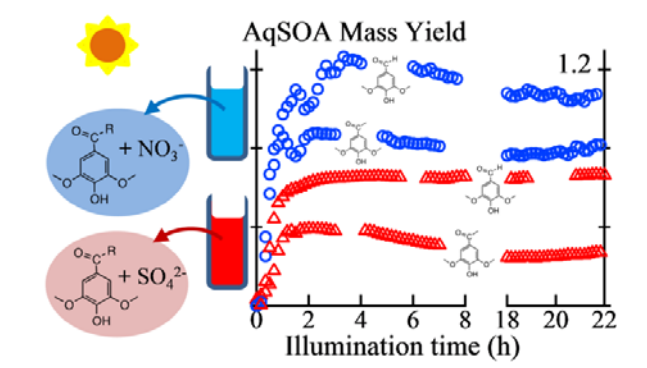
44

We investigate the effects of sulfate and nitrate on the formation and evolution of secondary organic aerosol formed in the aqueous phase (aqSOA) from photooxidation of two phenolic AqSOA was formed efficiently from the carbonyls emitted from wood burning. photooxidation of both syringaldehyde (C<sub>9</sub>H<sub>10</sub>O<sub>4</sub>) and acetosyringone (C<sub>10</sub>H<sub>12</sub>O<sub>4</sub>) in ammonium sulfate and ammonium nitrate solutions, with mass yields ranging from 30% to 120%. The initially formed aqSOA had oxygen-to-carbon (O/C) ratios and average carbon oxidation states (OSc) similar to the precursors, but much more oxidized aqSOA was formed over the course of photooxidiation, with O/C and OSc reaching 1.2 and 1.1, respectively. Positive matrix factorization on the organic mass spectra acquired by an Aerosol Mass Spectrometer revealed a combination of functionalization, oligomerization and fragmentation processes in the chemical evolution of aqSOA. Functionalization and oligomerization dominated in the first 4 hours of reaction, with phenolic oligomers and their derivatives significantly contributing to aqSOA formation. Oxidation of the first-generation products led to an abundance of oxygenated ring-opening products. Degradation rates of syringaldehyde and acetosyringone in nitrate solutions were 1.5 and 3.5 times faster than rates in sulfate solutions, and aqSOA yields in nitrate experiments are twice as high as in sulfate experiments. Nitrate likely promoted the reactions because it is a photolytic source of OH radicals, while sulfate is not. This work highlights the importance of aerosol-phase nitrate in the formation of aqSOA by facilitating the degradation of organic precursors.

- 45 Key words:
- 46 Phenolic carbonyls, photodegradation, aqueous phase reactions, nitrate and sulfate

47

# **TOC**



# 1 Introduction

Aqueous-phase oxidation reactions are important pathways for forming low-volatility products<sup>1-3</sup> and small dicarboxylic and keto acids in the atmosphere.<sup>3-6</sup> The fate of organic and inorganic constituents in clouds and fogs is strongly dependent on the composition of cloud/fog water.<sup>2-7</sup> Inorganic nitrate in cloud droplets/wet aerosols generates OH radicals and nitrating agents during illumination,<sup>8-10</sup> which can result in the formation of oligomers and nitro-organic components.<sup>11</sup> Nitrate-containing particles also effectively retain small organic acids even under dry conditions,<sup>12</sup> thereby increasing the oxidation state of aerosol particles.<sup>13</sup> In laboratory studies, sulfate is most often used as a representative inorganic species due to its ubiquity and abundance in ambient aerosol particles. However, nitrate is also the major component in aerosol particles and becoming increasingly important for the areas of significant reductions of SO<sub>2</sub> emission or of high ammonia emission due to increased population or agriculture use, where excess ammonia is available to neutralize the nitric acid.<sup>14,15</sup> Studies of the effects of inorganic nitrate on the formation and properties of SOA are limited to date.

Biomass burning emits large quantities of phenols and aromatic carbonyls (*e.g.*, aldehydes and ketones) of intermediate volatility and moderate water solubility (*e.g.*, Hozic et al., 2010<sup>16</sup> and references therein). Most previous studies have measured and chemically characterized the gas and particle emissions from biomass burning, while fewer have examined the fate and evolution of the emitted pollutants. Syringaldehyde (SyrAld, 4-hydroxy-3,5-dimethoxybenzaldeyhde, C<sub>9</sub>H<sub>10</sub>O<sub>4</sub>) and acetosyringone (ActSyr, 4'-hydroxy-3',5'-dimethoxyacetophenone, C<sub>10</sub>H<sub>12</sub>O<sub>4</sub>) are two examples of phenolic carbonyls released from the pyrolysis of lignin.<sup>17</sup> The structures of SyrAld and ActSyr differ by one methyl group and their vapor pressures are 6.49 × 10<sup>-5</sup> and 6.66 × 10<sup>-5</sup> mm Hg at 298 K,<sup>18</sup>

respectively. They both fall at the lower end of the intermediate volatility range (300 µg m<sup>-3</sup>  $< C^* < 3 \times 10^6 \,\mu g \, m^{-3})^{19}$  with saturation concentrations of approximately 700  $\mu g \, m^{-3}$ . SyrAld and ActSyr have high Henry's law constants of 4.39 x 10<sup>5</sup> and 1.13 x 10<sup>6</sup> M atm<sup>-1</sup>, respectively, at 298 K,18 and hence they partition favorably in the aqueous phase when liquid water is available.<sup>20,21</sup> Early ambient studies have indeed reported levels of micromolar concentrations of SyrAld in atmospheric waters.<sup>22,23</sup> Furthermore, these species undergo rapid direct photodegradation with lifetimes of 20 - 30 min in midday winter sunlight in Davis.<sup>24</sup> For these reasons, SyrAld and ActSyr can be important precursors of SOA through aqueous-phase reactions (aqSOA). However, there is little information on the reactions of phenolic carbonyls. Photo-oxidation of related compounds, such as phenol, catechol, syringol, guaiacol, toluene, etc., have been reported.<sup>25-32</sup> Reactions of the above mentioned compounds are dominated by radical-initiated reactions, such as hydroxylation of the aromatic ring through OH-radical addition. 26,29,33 Most recently, Pillar et al. (2014)34 found that heterogeneous oxidation of phenolic compounds, such as catechol, can efficiently form low volatility products as well as highly oxidized carboxylic acids. The reaction is initiated by electron transfer between ozone and the hydroxyl group on catechol, followed by the oxidation of the in-situ generated OH radicals. Triplet excited states of organic compounds (3C\*) is also found to be potentially important for the oxidation of phenolic compounds through H-abstraction from the hydroxyl group on the aromatic ring in both aqueous and gas phase.<sup>35</sup> It has been shown that aqSOA is formed from the reactions of phenol, guaiacol, and syringol with either 3C\* or OH radicals. <sup>26, 29</sup> H-abstraction from the substituent groups on the aromatic ring is generally minor. 36,37

75

76

77

78

79

80

81

82

83

84

85

86

87

88

89

90

91

92

93

94

95

96

97

98

99

In this work, we used a photoreactor to simulate the photooxidation of SyrAld and ActSyr in atmospheric cloud or fog droplets and investigate their potential contributions to the formation of aqSOA. We compare the aqSOA properties, yields and chemical

transformation of the tested compounds in ammonium sulfate or ammonium nitrate solutions to explore the potential effects of nitrate ions on SOA formation and evolution. Positive matrix factorization (PMF) analyses were also performed to examine the fates of SyrAld and ActSyr once dissolved in atmospheric waters after emission and the evolution of the produced aqSOA. Characteristic ions identified in this study might also serve as markers for aqSOA formed from biomass burning pollutants in ambient aerosols.

#### 2 Experiments and methods

## 2.1 Aqueous-phase reactions

Initial solutions of (1) 100 μM SyrAld or ActSyr in 22.7 μM ammonium sulfate (AS) or (2) 30 μM SyrAld or ActSyr in 200 μM ammonium nitrate (AN) were prepared; samples were adjusted to pH 5 with 5 μM sulfuric acid (H<sub>2</sub>SO<sub>4</sub>). For atmospheric relevance, the pH and initial concentrations of AS and AN are chosen based on the values observed in fog and cloud waters.<sup>38,39</sup> Ionic strength under both conditions was low (6.81\*10<sup>-5</sup> mol kg<sup>-1</sup> for AS and 20\*10<sup>-5</sup> mol kg<sup>-1</sup> for AN), thus is not expected to affect the chemical processes. Each solution was illuminated in stirred Pyrex tubes inside an RPR-200 photoreactor equipped with 16 light tubes, which are arranged symmetrically around the interior walls of a cylindrical reactor with a fan located at the bottom. The output of the tubes centered at approximately 315, 370, and 420 nm to mimic the sunlight; and the normalized distribution of the photon fluxes is shown in George et al. (2015).<sup>40</sup> Dark control samples were placed in a Pyrex tube wrapped in aluminum foil and kept in the same illumination chamber during the experiment. Each set of experiment contains measurements with one illumination tube and one dark tube for comparison.

Liquid samples were continuously aerosolized using N<sub>2</sub> or argon in a micro-concentric nebulizer (model SP8204B, Teledyne CETAC, Omaha, NE) coupled with a

cyclonic spray chamber (model 800-21, Analytical West, Inc., Lebanon, PA). The nebulized particles passed through a diffusion dryer before entering a high-resolution time-of-flight aerosol mass spectrometer (AMS; Aerodyne Res. Inc., Billerica, MA) for analysis. Online AMS measurements were made alternately between the illumination and dark tubes. For each set of experiments, UV illumination was turned on for 27 to 30 h. A three-way valve was employed to switch the sample flow from illumination tube to the dark tube for 45 to 60 min every 5-6 hours during the experiment. However since the residence time between the atomizer outlet and the AMS inlet was only ~ 15 s and the passage was in the dark, it is unlikely that the reactions, if occurred during this process, had played an important role in our experiments.

In the first 2 hours of illumination, offline samples were directly collected from the sample tubes using a syringe every 10 - 20 min and afterwards from the spray chamber in the form of drippings on an hourly basis. Concentrations of SyrAld or ActSyr in the solutions were measured using a high-performance liquid chromatograph (HPLC, ThermoScientific BetaBasic-18 C<sub>18</sub> column) with a UV-visible detector; wavelengths of 306 nm and 297 nm are selected for the detection of SyrAld and ASyr, respectively. The mobile phase consisted of 20:80 acetonitrile/water running at a flow rate of 0.7 mL min<sup>-1</sup>.<sup>28,29</sup> Organic anions, including formate, acetate, oxalate and malate, were analyzed with an Ion Chromatograph system (Metrohm 881 Compact IC Pro, Switzerland) as described in Ge et al. (2014).<sup>28</sup> Figure S1 shows an example of the IC chromatograms for standards and two of the offline samples. We note that some organic anions co-elute and cannot be separately quantified (e.g., oxalate and malate; Figure S1). Hence, we estimated the total concentrations of co-eluted organic anions using the average calibration coefficient and the lumped signal (Figure S1e).

#### 2.2 High-resolution aerosol mass spectrometric analysis

AMS has been widely employed in real time analysis of aerosol particles in both field and laboratory studies. <sup>41-44</sup> Details of the instrument have been described previously and its working principle is only briefly discussed here. <sup>45</sup> Aerosols sampled through an aerodynamic lens impact on a tungsten surface heated to 600 °C. The flash vaporized gaseous molecules were subsequently ionized by electron ionization (EI, 70eV), and the resultant positive ions are focused into a high-resolution time-of-flight mass spectrometer (mass resolution up to 5000). The universal and reproducible nature of 70eV EI ionization making quantification of non-refractory species possible, which can be used for a wide range of molecules, both inorganic as well as organic.

To capture the fast-changing properties of aqSOA, the AMS was operated in "V" mode (mass resolution of ~ 3000) at a high time-resolution of 0.5 min to acquire mass spectra up to m/z = 500. Standard AMS data analysis toolkits SQUIRREL v1.7 and PIKA 1.16 based on Igor Pro (6.37) were used to process the data. Based on our past work, the experimental setup effectively dries aerosols produced from aqueous reactions of phenols and methoxyphenols<sup>26</sup> and thus we assume no contributions from physically bound particulate or gas-phase water in the raw mass spectra. The organic H<sub>2</sub>O<sup>+</sup> signal was determined as the difference between the measured H<sub>2</sub>O<sup>+</sup> signal and that produced by sulfate.<sup>46</sup> The organic H<sub>2</sub>O<sup>+</sup> signal showed a good correlation with the measured CO<sub>2</sub><sup>+</sup> signal in both SyrAld and ActSyr experiments with ammonium sulfate (AS) (Figure S3a, SyrAld\_AS, r<sup>2</sup>= 0.98; Figure S3b, ActSyr\_AS, r<sup>2</sup>= 0.96). We therefore set H<sub>2</sub>O<sup>+</sup>= 0.55\*CO<sub>2</sub><sup>+</sup> and H<sub>2</sub>O<sup>+</sup>= 0.4\*CO<sub>2</sub><sup>+</sup> for the PIKA analyses of SyrAld and ActSyr in both AS and AN experiments, respectively. The signal intensities of OH<sup>+</sup> and O<sup>+</sup> were set based on the fragmentation pattern of water molecules for all experiments, *i.e.*, OH<sup>+</sup>= 0.25\*H<sub>2</sub>O<sup>+</sup> and O<sup>+</sup>= 0.4\*H<sub>2</sub>O<sup>+,46</sup>

In the illumination experiments of ActSyr\_AS where argon was used to atomize the solutions, the  $CO^+$  (m/z = 28) signal in the spectra of phenolic aqSOA was determined

directly by fitting the high resolution mass spectra (HRMS). The CO<sup>+</sup> signal showed a good correlation with the measured  $CO_2^+$  signal in the aqSOA (Figure S4,  $r^2 = 0.81$ ; Slope = 0.47). For experiments where  $N_2$  was used to atomize the solutions, direct quantification of  $CO^+$  was not possible because of the overwhelming long tail of the  $N_2$  signal.<sup>44</sup> Thus the  $CO^+$  signals in the aqSOA were scaled to the  $CO_2^+$  signals based on the relationship determined in the ActSyr\_AS experiment:  $CO^+ = 0.47*CO_2$ . Since  $H_xO^+$  and  $CO^+$  from aqSOA were directly quantified, the "Aiken-explicit" elemental analysis method was used to calculate the elemental ratios of the products.<sup>44,47</sup>

Pieber et al. (2016)<sup>48</sup> recently found that inorganic nitrate and sulfate salts can produce CO<sub>2</sub><sup>+</sup> ions when impinging on the heated tungsten vaporizer of the AMS due to the in-situ oxidation of pre-deposited refractory carbon. This portion of CO<sub>2</sub><sup>+</sup> is not generated by the organics in the particles (denoted by non-OA CO<sub>2</sub><sup>+</sup>), thus should be subtracted from the total AMS-detected CO<sub>2</sub><sup>+</sup> (denoted as CO<sub>2</sub><sup>+</sup>). The non-OA CO<sub>2</sub><sup>+</sup> was positively correlated with the nitrate-NO<sup>+</sup> signal<sup>48</sup> and was subtracted from the organic matrix in our nitrate experiments. The subtraction procedures are detailed in S-1 and the fragmentation table in PIKA was modified accordingly. After modifying fragmentation table, the mass spectrum for ActSyr in AN solutions were comparable to the standard mass spectrum of ActSyr in NIST database as shown in Figure S8, giving us confidence that the data processing and the method that applied to modify the fragmentation table are appropriate.

PMF analyses were performed for all experiments (see S-2). We generated the organic mass spectral matrices and the corresponding error matrices from both SQUIRREL and PIKA for ion fragments at *m/z* of 200-400 and 12-200 respectively. The error matrices were pretreated and the PMF results were evaluated using the PMF Evaluation Toolkit (PET, Version 2.06, <a href="http://cires1.colorado.edu/jimenez-group/wiki/index.php/PMF-AMS Analysis Guide">http://cires1.colorado.edu/jimenez-group/wiki/index.php/PMF-AMS Analysis Guide</a>). For each dataset, PMF results exhibit three distinct time series with

their corresponding mass spectral profiles. Selecting fewer or more factors than 3 will either lead to high residuals or over splitting of the factors. 3-factor PMF solutions were thus chosen for all the experiments and the results were carefully evaluated according to the procedures outlined in Zhang et al. (2011).<sup>50</sup>

#### 3 Discussions

#### 3.1 Overview of the aqSOA formation from phenolic carbonyls

Figure 1 provides an overview of the precursor decays and aqSOA yields (calculation detailed in S-3). Time series of elemental ratios for all four types of illumination experiments were shown in Figure S7 and a table of experiments with the list of all parameters is also summarized to the supporting information, Table-S1. As illustrated in Figures 1a and 1b, upon illumination, phenolic carbonyls rapidly degraded in both AN and AS experiments. The reactions followed apparent first-order kinetics reasonably well and apparent first-order rate constants (k') for loss were determined using Eq. (1):

$$ln\left(\lceil PhC\rceil_{\bullet}/\lceil PhC\rceil_{0}\right) = -k't \tag{1}$$

where  $[PhC]_t$  and  $[PhC]_0$  are the concentrations of the phenolic carbonyls measured by HPLC at time t and 0, respectively. There was no significant loss (over 24 hr) of the precursors in the dark control experiments (Figure S2).

In ammonium sulfate solutions, the rate constants for decay of SyrAld and ActSyr were  $0.87 \times 10^{-3} \text{ s}^{-1}$  and  $0.41 \times 10^{-3} \text{ s}^{-1}$ , respectively; this difference is likely due to the greater light absorption by SyrAld.<sup>24</sup> In contrast, in ammonium nitrate solutions the rate constants for SyrAld and ActSyr were faster and essentially the same, with k' values of  $1.3 \times 10^{-3} \text{ s}^{-1}$  and  $1.4 \times 10^{-3} \text{ s}^{-1}$ , respectively. This enhancement is likely due to nitrate photolysis forming hydroxyl (OH) radical (*e.g.*, Benedict et al., 2017),<sup>51</sup> which reacts very rapidly with

phenols.<sup>52</sup> Gas-phase reaction rate constants between SyrAld/ActSyr and OH radicals are not available. Rate constant of a similar compound, vanillin, has been reported previously  $(10\times10^{-11}~{\rm cm^3}~{\rm molecules^{-1}~s^{-1}})$ .<sup>52</sup> Assuming a gas-phase OH concentration of  $1\times10^6~{\rm cm^3}$  molecules<sup>-1</sup>,<sup>53</sup> gas-phase oxidation of loss rates of SyrAld/ActSyr would be on the order of  $1\times10^{-4}~{\rm s^{-1}}$ . The apparent loss rates in our experiments are on the order of  $10^{-4}~{\rm s^{-1}}$  in sulfate solution and  $10^{-3}~{\rm s^{-1}}$  in nitrate solution, which are comparable to or larger than the gas-phase loss rate, suggesting that aqueous-phase chemistry is likely to be at least as important as gas-phase chemistry for phenolic carbonyls. It should also be noted that the phenolic carbonyl concentrations in the AS (100  $\mu$ M) experiments were much higher than those in AN (30  $\mu$ M), resulting in decreased volume-averaged photon fluxes due to the screening of light; this might also contribute to the slower precursor decay in AS experiments.

The AMS quantification of aqSOA mass concentrations ( $\mu$ g/m³) were converted to concentrations ( $\mu$ g L¹¹) in the solution using inorganic sulfate as an internal standard. As shown in Figures 1c and 1d, the aqSOA mass yield, *i.e.*, the ratio of the aqSOA mass formed to the mass of phenol precursor reacted, increased dramatically as soon as illumination started. The prompt formation of aqSOA is probably due to fast functionalization and oligomerization reactions, which form lower volatility oxidized organic species, such as aromatic derivatives and oligomers. <sup>21,26</sup> <sup>29,34</sup> This hypothesis is consistent with the increase of H/C and O/C ratios (Figures S7a – 7d), supporting the formation of functionalized products, likely through hydroxylation or other oxygenation pathways. Note that H/C, O/C and OS<sub>C</sub> are not reported for the first 15 min of the reactions because the aqSOA masses were too low, making the elemental ratios highly uncertain. The aqSOA mass reached a plateau in all the experiments at t = 2 h, when essentially all of the precursor was consumed. Yet, interestingly, the yields of aqSOA in AN are twice as high as those in the AS experiments, indicating that AN promoted not only the degradation of precursors but also the production of aqSOA. In

addition, the O/C of the aqSOA in AS experiments increased continuously in the first 2 hours of reactions, while those in AN experiments first increased and then decreased, with the O/C of aqSOA from both experiments converging to an end value of ~ 0.85. As shown in Figure 1, in the AN experiments approximately half of the phenolic carbonyl was consumed within 30 min, and near the same time the O/C ratios of the aqSOA were peaking at 1.2 (for SyrAld) or 0.9 (for ActSyr), suggesting that the highly oxidized products were formed quickly and then decomposed in AN experiments.

Overall, the carbon oxidation state (OS<sub>C</sub> =  $2 \times O/C$  - H/C) of the formed aqSOA after approximately 2 h was ~ 0.3 for both phenolic carbonyls, much higher than the precursor compounds (- 0.2 and - 0.4 for SyrAld and ActSyr, respectively) (Figures S1e and 1f). These increases of OS<sub>C</sub> ( $\Delta$ OS<sub>C</sub> ~ 0.5 - 0.8) are comparable to the  $\Delta$ OS<sub>C</sub> ( $\sim$  0.8 - 1.1) observed for aqSOA formed by the oxidation of phenol and methoxyphenols by triplet excited states ( $^3$ C\*) and hydroxyl radicals.  $^{21,26,29}$  The large increases in OS<sub>C</sub> for phenolic aqSOA demonstrate that aqueous processing of VOCs from biomass burning emissions could be an important source of oxygenated species in the atmosphere.

#### 3.2 Chemical evolution of phenolic aqSOA

As shown in Figure 1, the bulk chemical composition aqSOA appeared to have changed significantly during the first four hours of illumination but is relatively stable afterwards. To more clearly assess the chemical evolution of the aqSOA, we next examined the time course of factors determined from PMF. The time series and the corresponding mass spectral profiles of the 3-factor PMF solution are presented in Figures 2. Characteristic ions, if identifiable for each factor, provide important insights into reaction processes and mechanisms. Hence, we calculated the relative contribution of each factor to individual ions as shown in Figure S6. Thus, the characteristic ions are those dominated by a certain factor.

# 3.2.1 Initial growth of aqSOA

Numerous studies have utilized PMF to analyze AMS data for source apportionment
in field studies <sup>49,50,54</sup> and chemical evolution and conversions of aerosol particles in
laboratory studies. 13,55 Here, we use PMF to deconvolve the AMS measured OA spectral
matrix; each resolved PMF factor represents a group of molecules with similar
chemical/physical properties resulting from oxidation and gas-particle partitioning (during
evaporation) processes, which evolved as reaction went on. For all four experiments, Factor 1
increased the most dramatically during the first hour of reactions (Figure 2). 90% of SyrAld
and 70% of ActSyr in the AS experiments were degraded by $t = 1h$ when Factor $1_{SyrAld\_AS}$ and
Factor 1 <sub>ActSyr_AS</sub> reached their peaks, indicating the rapid transformation of precursors to low-
volatility compounds (i.e., aqSOA). Precursor ions, SyrAld (C <sub>9</sub> H <sub>9</sub> O <sub>4</sub> <sup>+</sup> ; $m/z = 181$ ) or ActSyr
$(C_{10}H_{12}O_4^+; m/z = 196)$ can be clearly observed in the mass spectra of Factor $1_{SyrAld\_AS}$ and
Factor 1 <sub>ActSyr_AS</sub> and their degradation profiles resembled those of the HPLC-measured
precursors (Figures 3a and 3b). Besides the precursor-related ions, ions at $m/z = 125$
$(C_6H_5O_3^+)$ , 153 (primarily $C_7H_5O_4^+$ ), 167 $(C_8H_7O_4^+)$ , 168 $(C_8H_8O_4^+)$ and 170 $(C_7H_6O_5^+)$ are
also the major peaks in the mass spectrum of Factor $1_{SyrAld\_AS}$ (Figure 2b). $C_8H_8O_4^+$ ( $m/z$ 168)
and C <sub>7</sub> H <sub>6</sub> O <sub>5</sub> <sup>+</sup> (m/z 170) are likely produced from the de-methylated monomeric products of
SyrAld (Scheme 1); $^{29,30}$ and $C_6H_5O_3^+$ ( $m/z$ 125) and $C_7H_5O_4^+$ ( $m/z$ 153) are their major
electron ionization products (see the NIST spectra of 3,4-dihydroxy-5-methoxybenzaldehyde
$(C_8H_8O_4)$ and 3,4,5-trihydroxybenzoic acid $(C_7H_6O_5)$ in Figures S9 and S10). Ions that
indicate the presence of hydroxylated or oxygenated monomers, i.e., $C_9H_{10}O_5^+$ ( $m/z = 198$ )
and $C_7H_6O_4^+$ ( $m/z = 154$ ), were also observed primarily in Factor 1 <sub>SyrAld_AS</sub> (Figure 2b).

Furthermore, ions in the mass range of 200 – 400 Da are observed (Figure 2b) in the Factor 1 of the SyrAld\_AS, SyrAld\_AN and ActSyr\_AN experiments. Clusters of peaks are regularly separated by mass units of 14 - 18 Da, which is a characteristic of copolymer

systems.<sup>56,57</sup> For example, a series of ions suggesting SyrAld oligomers with  $\Delta$  m/z = 14 is identified in Figure 2b. The regular mass intervals of 14, 16, and 18 Da indicate the difference in CH<sub>2</sub>, O, and H<sub>2</sub>O groups, respectively, among the oligomers/clusters, consistent with numerous combinations of monomer units with multiple sites of oxidation (alcohols, ethers, carbonyls, and acids). Although both monomeric derivatives and oligomeric products contributed to the increased organic mass and OS<sub>C</sub> in the first 2 hours of the reactions, functionalization processes, such as hydroxylation and oxygenation, were likely more important than oligomerization processes. This is shown in the Van Krevelen diagrams for the aqSOA from SyrAld\_AS and ActSyr\_AS experiments (Figure 4a), where the O/C and H/C ratios simultaneously increase, with nearly linear relationships, during the first 2 hours of reactions.

#### 3.3.2 Formation of high molecular weight (HMW) products

At reaction times longer than 2 hours, Factor 2 reached its highest concentrations and oligomers became important components. Factor 2 contributed most to the abundance of the HMW ions (m/z > 160) (Figure S6). Both H/C and O/C ratios decreased at illumination times longer than 2 h (Figure 4), likely resulting from oligomerization via elimination of H<sub>2</sub>O.<sup>26,29</sup> This converts the functionalized products in Factor 1 to the HMW products in Factor 2 without much change in overall aqSOA yields. Factor 2 began decreasing approximately 4 hours after the start of illumination. This is accompanied by an increase of Factor 3, which had smaller fractions of HMW ions than Factor 2, likely due to the decomposition of the HMW products in Factor 2 (Figure S6). Distinctive peaks at m/z 121 (C<sub>7</sub>H<sub>5</sub>O<sub>2</sub><sup>+</sup>, proposed structure in Figure S11) in Factor 3 (Figure 2) are likely generated from the decomposed phenol esters or the monomeric intermediates upon cleaving the methoxy functional groups.<sup>29,58</sup>

Though fragmentation of previously formed oligomers is significant after six hours of illumination, ions representing dimers (e.g.,  $C_{17}H_{18}O_{8}^{+}$  at m/z = 350 and  $C_{17}H_{18}O_{7}^{+}$  at m/z = 334; Figure S12) keep increasing since the beginning of illumination and show good correlations with Factor 3 (Figure 3d).  $C_{17}H_{18}O_{8}^{+}$  and  $C_{17}H_{18}O_{7}^{+}$  represent the largest peaks in the spectra of both Factor  $3_{SyrAld\_AS}$  and Factor  $3_{ActSyr\_AS}$  above 200 Da (Figures 2b and 2d). Since these ions have an odd number of electrons with relatively high m/z values, they are likely the respective molecular compounds with the loss of one electron ([M -  $e^{-r}$ ]+) instead of the ionization fragments.  $^{29,59}$  Molecular characterization of samples should be conducted in the future. Scheme 1 illustrates the formation of dimeric compounds, which involves the formation of a quinoide-type intermediate  $^{60}$  followed by the elimination of carbonyl group. The presence of dimers in both Factors 2 and 3 suggests that oligomers formed via multiple pathways during the aqueous-phase photooxidation of the phenolic carbonyls. The oligomers formed in Factor 2 might have come from the coupling of phenoxy radicals  $^{26}$  while those formed later in Factor 3 likely involved the formation of the quinoide-type intermediates.

#### 3.3.3 Competition between oligomerization and fragmentation

A higher fraction of HMW ions (m/z>160) were observed in Factor 2 than in Factor 3, suggesting that HMW products were largely formed at intermediate steps in the reaction while decomposition was more significant during the later stage of the reactions. In all experiments, Factor 3 contributed significantly to the small molecular weight ions (m/z < 100, Figure 2) including some that are highly oxygenated, e.g., m/z 47 (CH<sub>3</sub>O<sub>2</sub><sup>+</sup>), 77 (C<sub>2</sub>H<sub>5</sub>O<sub>3</sub><sup>+</sup>). The simultaneous growth of small oxygenates and oligomeric products in Factor 3 (Figure 3d) indicates that fragmentation competed with oligomerization, especially after 12 hours postillumination.

We also see evidence for ring-opening reactions from the ion chromatography (IC) detection of small organic acids, *e.g.*, oxalic acid (Figure 5), which is an important oxidation product from the decomposition of larger molecular weight precursors in aqueous aging processes. <sup>21,26,61</sup> Oxalic and malic acid concentrations generally increased throughout illumination, at least to a small extent, for both precursors (Figures 5a and 5b), which is an indication of oxidative aging. Based on all of our analyses, functionalization and oligomerization processes were major processes contributing to the growth of the SOA mass during the first 4 hours of illumination. At later times fragmentation became increasingly important, leading to the decomposition of the previously formed oligomers and the formation of smaller oxygenated products.

#### 3.3.4 Comparison between AN and AS experiments

In IC analyses, higher concentrations of organic acids were detected in AN experiments compared to AS experiments (Figures 5a-b). This difference suggests that oxidation-induced fragmentation was more prevalent in AN than in AS experiments, especially during the later stages of the reactions. Note that the samples analyzed by IC were the solutions collected directly from the dripping line of the atomizer. Thus, the IC results include volatile and semivolatile organic acids as well. It is also possible that particles from the AN experiment may retain more water and more water-soluble VOCs in the aerosol-phase than from the AS experiment. However, no water was detected in the AN particles generated using the same atomization and drying setup.

From PMF analysis, the mass spectra of the corresponding factors in AN and AS experiments share similar characteristic patterns and ions. For example, the cluster distributions, characteristic dimeric ions (m/z 350, 376 and 394) and characteristic ions from decomposed oligomers (m/z 121) observed in AS experiments were also present in AN

experiments (Figure 2). On the other hand, precursor ions were barely observed in the spectra of Factor 1\_SyrAld\_AN and Factor 1\_ActSyr\_AN due to the rapid degradation of the precursor compounds in nitrate solution. Dimeric ions, including those at m/z = 350, 376 and 394, which were only present after 4 hours of reactions in SyrAld\_AS and ActSyr\_AS, were formed within 30 min of reactions in SyrAld\_AN and ActSyr\_AN (Figure S13). Overall, the similarity in the characteristic ions in AN and AS experiments suggests that the reaction pathways, *i.e.*, functionalization, fragmentation, and oligomerization, can be similar in both conditions. Yet, the reactions were much faster and more extensive in AN than in AS experiments. Furthermore, the higher concentrations of organic acids and the overall more oxidized aqSOA from AN experiments compared to AS experiments suggest that the photolysis of AN was a source of oxidants that led to faster oxidations of phenolic carbonyls and higher aqSOA yields. Note that the signals of NO<sup>+</sup> and NO<sub>2</sub><sup>+</sup> in particles measured by the AMS showed tight correlation throughout the entire AN experiments and the linear regression slope of signal ratio of NO<sup>+</sup>/NO<sub>2</sub><sup>+</sup> was very similar to that of AN, suggesting that there was no significant organonitrate formation in the AN experiments.

## 4 Implications

This work demonstrates that UV irradiation of SyrAld and ActSyr (separately) in aqueous phase can form low-volatility aqSOA composed of more oxidized and larger molecules compared to the precursors. Reactions of phenolic compounds are dominated by radical-initiated reactions, such as hydroxylation of the aromatic ring through OH-radical addition. And a larger molecules compared to the precursors. Reactions of phenolic compounds are dominated by radical-initiated reactions, such as hydroxylation of the aromatic ring through OH-radical addition. And a larger molecules compared to the precursors. The formation of the aromatic ring through of the aromatic ring, e.g. alkyl groups, is generally minor. The formation of aqSOA in this study was initiated by direct photodegradation, or the in-situ generated oxidants, e.g., OH radicals or triple excited states of organic compounds (3C\*), which are efficiently generated through aqueous-phase photolysis of inorganic nitrate or aromatic carbonyls. Previous studies have also

shown that aqSOA is formed from the reactions of phenol, guaiacol, and syringol with either  ${}^{3}C^{*}$  or OH radicals. ${}^{26,29}$ 

After the initial phase of reaction, the intermediates react to form ring-opening and ring-retaining products. 62 Fragmentation competes with oligomerization and functionalization for both precursors, especially during the later course of the experiments, leading to the formation of highly oxygenated products. Comparing ActSyr and SyrAld, which have different moieties on the aromatic ring, SyrAld (with –CHO as substituent) generates more aqSOA than ActSyr (with –C(O)CH<sub>3</sub>). More extensive ring-opening reactions were found to occur in AN than in AS solutions. Li et al. (2014)<sup>21</sup> showed that the branching ratios of oligomerization and fragmentation may be altered by the concentration ratios between oxidants and organic precursors. In this work, although both small oxygenates and oligomers were observed in AN and AS experiments, the more extensive fragmentation of aqSOA in AN than in AS experiments is consistent with a higher steady-state concentration of OH radicals in the former. The aqueous-phase processing of phenolic compounds in the presence of nitrate enhanced the formation of carboxylic acids, and thus might be an important source of the small acids detected in ambient aerosols.

Further experiments should be directed to determine the kinetics of organic degradation for a variety of aqSOA precursors in nitrate-containing solutions or particles, which can be used in aqSOA-predictive models and in estimating the lifetimes of biomass-burning products. The identification and quantification of products at the molecular level will improve the understanding of the quantitative impact of nitrate on the formation mechanisms of aqSOAs during cloud processing, via pathways such as OH radical generation and the formation of organic nitrate.

#### **Acknowledgements**

The UC Davis groups acknowledge financial support of the US National Science Foundation, (grants. AGS-1036675 and AGS-1649212) and the US Department of Energy, Atmospheric System Research (ASR) program (grant DE-SC0014620). Heidi H.Y. Cheung acknowledges the HKUST overseas research award. Dan Dan Huang and Chak K. Chan acknowledge the financial support of the startup fund of the City University of Hong Kong. We also want to thank Dr. Sonya Collier (UC Davis, now at California Air Resources Board) for offering helps during the experiments.

# **Supporting Information**

- The supporting information includes additional information as noted in the text:
- S-1, Subtraction of non-OA CO<sub>2</sub>+; S-2, PMF analysis; S-3,aqSOA yields; Figures S1-S15;
- 426 Table S1.
- This information is available free of charge via the Internet at http://pubs.acs.org.

#### References:

- 429 (1) Blando, J. D.; Turpin, B. J. Secondary organic aerosol formation in cloud and fog
- droplets: a literature evaluation of plausibility. *Atmos. Environ.* **2000**, *34*(10), 1623–1632.
- 431 (2) Ervens, B. Modeling the Processing of Aerosol and Trace Gases in Clouds and Fogs.
- 432 *Chem. Rev.* **2015**, *115*(10), 4157–4198.
- 433 (3) Alexis J. Eugene, Marcelo I. Guzman, Reactivity of ketyl and acetyl radicals from direct
- 434 solar actinic photolysis of aqueous pyruvic acid. J. Phys. Chem. A 2017, 121, 2924–2935.
- 435 (4) Altieri, K. E.; Carlton, A. G.; Lim, H. J.; Turpin, B. J. and Seitzinger, S. P. Evidence for
- 436 oligomer formation in clouds: reactions of isoprene oxidation products, Environ. Sci.
- 437 *Technol.* **2006**, 40, 4956–4960.
- 438 (5) Baboukas, E. D.; Kanakidou, M.; Mihalopoulos, N. Carboxylic acids in gas and
- particulate phase above the Atlantic Ocean, J. Geophys. Res. 2000, 105, 2156-2202.
- 440 (6) Charbouillot, T.; Gorini, S.; Voyard, G.; Parazols, M.; Brigante, M.; Deguillaume, L.;
- Delort, A.; Mailhot, G. Mechanism of carboxylic acid photooxidation in atmospheric aqueous
- phase: Formation, fate and reactivity. Atmos. Environ. 2012, 56, 1352-2310.
- 443 (7) Passananti, M.; Vinatier, V.; Delort, A.-M.; Mailhot, G.; Brigante, M. Siderophores in
- 444 cloud waters and potential impact on atmospheric chemistry: Photoreactivity of iron
- complexes under sun-simulated conditions. Environ. Sci. Technol. 2016, 50 (17), 9324–9332.
- 446 (8) Herrmann, H.; Tilgner, A.; Barzaghi, P.; Majdik, Z.; Gligorovski, S.; Poulain, L.; Monod,
- 447 A.; Towards a more detailed description of tropospheric aqueous phase organic chemistry:
- 448 CAPRAM 3.0, Atmos. Environ. **2005**, 39, 4351-4363.
- 449 (9) Vione, D.; Maurino, V.; Minero, C.; Pelizzetti, E.; Harrison, M. A. J.; Olariu, R.-I.;
- 450 Arsene, C. Photochemical reactions in the tropospheric aqueous phase and on particulate
- 451 matter. Chem. Soci. Rev. 2006, 35(5), 441–453.
- 452 (10) Scharko, N. K.; Berke, A. E.; Raff, J. D. Release of Nitrous Acid and Nitrogen Dioxide
- 453 from Nitrate Photolysis in Acidic Aqueous Solutions. Environ. Sci. Technol. 2014, 48(20),
- 454 11991–12001.
- 455 (11) Minero, C.; Bono, F.; Rubertelli, F.; Pavino, D.; Maurino, V.; Pelizzetti, E.; Vione, D.
- On the effect of pH in aromatic photonitration upon nitrate photolysis. Chemosphere. 2007,
- 457 66, 650-656.
- 458 (12) Shilling, J. E.; Connelly, B. M.; Tolbert, M. A. Uptake of small oxygenated organic
- molecules onto ammonium nitrate under upper tropospheric conditions. J. Phys. Chem. A.
- **2006**, 110(21), 6687–6695.
- 461 (13) Huang, D. D.; Zhang, X.; Dalleska, N. F.; Lignell, H.; Coggon, M. M.; Chan, C.-M.;
- 462 Chan, C. K. A note on the effects of inorganic seed aerosol on the oxidation state of
- 463 secondary organic aerosol- α -Pinene ozonolysis. J. Geophys. Res. Atmos., 2016, 121(20),
- 464 12,476-12,483.
- 465 (14) West, J.J., Ansari, A.S., Pandis, S.N. Marginal PM2.5: nonlinear aerosol mass response
- to sulfate reductions in the Eastern United States. J. Air Waste Manag. Assoc. 1999,49 (12),
- 467 1415-1424.
- 468 (15) Myhre, G.; Shindell, D.; Bréon, F.-M.; Collins, W.; Fuglestvedt, J.; Huang, J.; Koch, D.;
- 469 Lamarque, J.-F.; Lee, D.; Mendoza, B.; Nakajima, T.; Robock, A.; Stephens, G.; Takemura,
- 470 T.; and Zhang, H. Anthropogenic and Natural Radiative Forcing, in: Climate Change 2013:

- 471 The Physical Science Basis, Contribution of Working Group I to the Fifth Assessment Report
- of the Inter- governmental Panel on Climate Change, edited by: Stocker, T. F.; Qin, D.;
- Plattner, G.-K.; Tignor, M.; Allen, S. K.; Boschung, J.; Nauels, A.; Xia, Y.; Bex, V.; and
- 474 Midgley, P. M. Cambridge University Press, Cambridge, UK and New York, NY, USA, 659-
- 475 740, **2013**b.
- 476 (16) Hodzic, A.; Jimenez, J. L.; Madronich, S.; Canagaratna, M. R.; DeCarlo, P. F.;
- 477 Kleinman, L.; Fast, J. Modeling organic aerosols in a megacity: potential contribution of
- 478 semi-volatile and intermediate volatility primary organic compounds to secondary organic
- 479 aerosol formation. Atmos. Chem. Phys. **2010**, 10(12), 5491–5514.
- 480 (17) Schauer, J. J.; Kleeman, M. J.; Cass, G. R. and Simoneit, B. R.T. Measurement of
- 481 Emissions from Air Pollution Sources. 3. C1-C29 Organic Compounds from Fireplace
- 482 Combustion of Wood, *Environ. Sci. Technol.* **2001**, 35 (9), 1716-1728.
- 483 (18) Estimation Programs Interface Suite<sup>TM</sup> for Microsoft® Windows, v 4.1. United States
- Environmental Protection Agency, Washington, DC, USA, 2012.
- 485 (19) Robinson, A. L.; Donahue, N. M.; Shriyastava, M. K.; Weitkamp, E.; Sage, A. M.;
- 486 Grieshop, A. P.; Pandis, S. N. Rethinking Organic Aerosols. *Science*, **2007**, *315*, 1259–1262.
- 487 (20) Ip, H. S. S., Huang, X. H. H., and Yu, J. Z. Effective Henry's law constants of glyoxal,
- 488 glyoxylic acid, and glycolic acid, *Geophys. Res. Lett.* **2009**, 36, L01802.
- 489 (21) Li, Y. J.; Huang, D. D.; Cheung, H. Y.; Lee, A. K. Y.; Chan, C. K. Aqueous-phase
- 490 photochemical oxidation and direct photolysis of vanillin a model compound of methoxy
- 491 phenols from biomass burning. *Atmos. Chem. Phys.* **2014**,14(6), 2871–2885.
- 492 (22) Hawthorne, S. B.; Miller, D. J.; Langenfeld, J. J. and Krieger, M.S. PM-10 high-volume
- 493 collection and quantitation of semi- and nonvolatile phenols, methoxylated phenols, alkanes,
- and polycyclic aromatic hydrocarbons from winter urban air and their relationship to wood
- 495 smoke emissions, *Environ. Sci. Technol.* **1992**, 26, 2251–2262.
- 496 (23) Sagebiel, J. C; Seiber, J. N. Studies on the occurrence and distribution of wood smoke
- 497 marker compounds in foggy atmospheres, *Environ. Toxicol. Chem.* **1993**, 12, 813–822.
- 498 (24) Smith, J. D.; Haley K.; Cort, A. Phenolic carbonyls undergo rapid aqueous
- 499 photodegradation to form low-volatility, light-absorbing products. Atmos. Environ. 2016,126,
- 500 36–44.
- 501 (25) Canonica, S., Hellrung, B., Wirz, J. Oxidation of phenols by triplet aromatic ketones in
- 502 aqueous solution. J. Phys. Chem. A 2000, 104, 1226e1232.
- 503 (26) Sun, Y. L.; Zhang, Q.; Anastasio, C.; Sun, J. Insights into secondary organic aerosol
- 504 formed via aqueous-phase reactions of phenolic compounds based on high resolution mass
- 505 spectrometry. Atmos. Chem. Phys. **2010**. 10(10), 4809–4822.
- 506 (27) Clifford, G. M., A. Hadj-Aissa, R. M. Healy, A. Mellouki, A. Munoz, K. Wirtz, M.
- Martin Reviejo, E. Borras, and J. C. Wenger, The Atmospheric Photolysis of o-Tolualdehyde,
- 508 Environ. Sci. Technol. 2011, 45(22), 9649-9657.
- 509 (28) Smith, J. D.; Sio, V.; Yu, L.; Zhang, Q.; Cort, A. Secondary Organic Aerosol Production
- 510 from Aqueous Reactions of Atmospheric Phenols with an Organic Triplet Excited State.
- 511 Environ. Sci. Technol. 2014, 48(2), 1049–1057.
- 512 (29) Yu, L.; Smith, J.; Laskin, A.; Anastasio, C.; Laskin, J.; Zhang, Q. Chemical
- 513 characterization of SOA formed from aqueous-phase reactions of phenols with the triplet
- excited state of carbonyl and hydroxyl radical. Atmos. Chem. Phys. 2014,14(24), 13801–

- 515 13816.
- 516 (30) Yu, L.; Smith, J.; Laskin, A.; George, K. M.; Anastasio, C.; Laskin, J.; Zhang, Q.
- 517 Molecular transformations of phenolic SOA during photochemical aging in the aqueous
- 518 phase: competition among oligomerization, functionalization, and fragmentation. Atmos.
- 519 Chem. Phys. **2016**,16(7), 4511–4527.
- 520 (31) Pillar, E. A.; Zhou, R.; Guzman, M. I. Heterogeneous oxidation of catechol. J. Phys.
- 521 *Chem. A* **2015**, 119 (41), 10349–10359.
- 522 (32) Pillar, E. A.; Zhou, R.; Guzman, M. I. Oxidation of substituted catechols at the air-water
- 523 interface: production of carboxylic acids, quinones, and polyphenols. Environ. Sci. Technol.,
- **2017**, 51 (9), 4951–4959.
- 525 (33) Ziemann, P. J.; Atkinson, R. Kinetics, products, and mechanisms of secondary organic
- 526 aerosol formation, *Chem. Soc. Rev.* **2012**, 41, 6582-6605.
- 527 (34) Pillar, E. A.; Camm, R. C.; Guzman, M. I. Catechol oxidation by ozone and hydroxyl
- 528 radicals at the air-water interface. Environ. Sci. Technol. 2014, 48 (24), 14352–14360.
- 529 (35) Matsushita, Y., Y. Yamaguchi, and T. Hikida, The photochemical reaction of excited
- acetophenone and benzaldehyde in the gas phase, *Chem. Phys.* **1996**, 213(1-3), 413-419.
- 531 (36) Coeur-Tourneur, C.; Tomas, A.; Guilloteau, A.; Henry, F.; Ledoux, F.; Visez, N.;
- Riffault, V.; Wenger, J. C.; Bedjanian, Y. Aerosol formation yields from the reaction of
- 533 catechol with ozone, *Atmos. Environ.* **2009**, 43, 2360–2365.
- 534 (37) Yee, L. D.; Kautzman, K. E.; Loza, C. L.; Schilling, K. A.; Coggon, M. M.; Chhabra, P.
- 535 S.; Chan, M. N.; Chan, A. W. H.; Hersey, S. P.; Crounse, J. D.; Wennberg, P. O.; Flagan, R.
- 536 C.; Seinfeld, J. H. Secondary organic aerosol formation from biomass burning intermediates:
- phenol and methoxyphenols, *Atmos. Chem. Phys.* **2013**,13, 8019-8043.
- 538 (38) Jeffrey L. Collett, Katherine J. Hoag, D.Eli Sherman, Aaron Bator, L.Willard Richards,
- 539 Spatial and temporal variations in San Joaquin Valley fog chemistry, Atmos. Environ., 1998,
- 540 33 (1), 129-140.
- 541 (39) Fahey, K. M., Pandis, S. N., Collett, J. L., Herckes, P., The influence of size-dependent
- droplet composition on pollutant processing by fogs, Atmos. Environ., 2005, 39 (25), 4561-
- 543 4574.
- 544 (40) George, K. M.; Ruthenburg, T. C.; Smith, J.; Yu, L.; Zhang, Q.; Anastasio, C.; Dillner,
- 545 A. M. FT-IR quantification of the carbonyl functional group in aqueous-phase secondary
- organic aerosol from phenols. *Atmos. Environ.* **2015**, 100, 230–237.
- 547 (41) Canagaratna, M., Jayne, J., Jimenez, J., Allan, J., Alfarra, M., Zhang, Q., Onasch, T.,
- 548 Drewnick, F., Coe, H., Middlebrook, A., Delia, A., Williams, L., Trimborn, A., Northway,
- M., DeCarlo, P., Kolb, C., Davidovits, P. and Worsnop, D. Chemical and microphysical
- characterization of ambient aerosols with the aerodyne aerosol mass spectrometer. Mass
- 551 Spectrom. Rev. 2007, 26: 185-222.
- 552 (42) Zhang, Q., et al., Ubiquity and dominance of oxygenated species in organic aerosols in
- 553 anthropogenically-influenced Northern Hemisphere midlatitudes. Geophys. Res.
- 554 *Lett.***2007**, 34, L13801.
- 555 (43) Jimenez et al., Evolution of Organic Aerosols in the Atmosphere, *Science*, 2009, 326,
- 556 1525-1529.
- 557 (44) Aiken, A. C.; DeCarlo, P. F.; Kroll, J. H.; Worsnop, D. R.; Huffman, J. A.; Docherty, K.
- 558 S.; Jimenez, J. L. O/C and OM/OC Ratios of Primary, Secondary, and Ambient Organic

- 559 Aerosols with High-Resolution Time-of-Flight Aerosol Mass Spectrometry, Environ. Sci.
- 560 *Technol.*, **2008**, 42(12), 4478–4485.
- 561 (45) DeCarlo, P. F., Kimmel, J. R., Trimborn, A., Northway, M. J., Jayne, J. T., Aiken, A. C.,
- 562 ... Jimenez, J. L. Field-deployable, high-resolution, time-of-flight aerosol mass spectrometer.
- 563 Anal Chem. **2006**, 78(24), 8281–8289.
- 564 (46) Allan, J. D.; Delia, A. E.; Coe, H.; Bower, K. N.; Alfarra, M. R.; Jimenez, J. L.;
- Worsnop, D. R. A generalised method for the extraction of chemically resolved mass spectra
- from aerodyne aerosol mass spectrometer data. J. Aerosol Sci., 2004. 35(7), 909–922.
- 567 (47) Aiken, A. C.; DeCarlo, P. F.; Jimenez, J. L. Elemental analysis of organic species with
- 568 electron ionization high-resolution mass spectrometry, Anal. Chem., 2007, 79(21), 8350–
- 569 8358.
- 570 (48) Pieber, S. M.; El Haddad, I.; Slowik, J. G.; Canagaratna, M. R.; Jayne, J. T.; Platt, S. M.;
- 571 Prévôt, A. S. H. Inorganic Salt Interference on CO <sub>2</sub> + in Aerodyne AMS and ACSM Organic
- 572 Aerosol Composition Studies. Environ. Sci. Technol. 2016, 50(19), 10494–10503.
- 573 (49) Ulbrich, I. M.; Canagaratna, M. R.; Zhang, Q.; Worsnop, D. R.; Jimenez, J. L.
- 574 Interpretation of organic components from Positive Matrix Factorization of aerosol mass
- 575 spectrometric data. Atmos. Chem. and Phys. **2009**, 9(9), 2891–2918.
- 576 (50) Zhang, Q.; Jimenez, J.; Canagaratna, M.; Ulbrich, I.; Ng, N.; Worsnop, D.; Sun, Y.
- 577 Understanding atmospheric organic aerosols via factor analysis of aerosol mass spectrometry:
- 578 a review. Analy. Bioanaly. Chem. **2011**, 401(10), 3045–3067.
- 579 (51) Benedict K. B.; McFall A.S.; Anastasio C. Quantum Yield of Nitrite from the Photolysis
- 580 of Aqueous Nitrate above 300 nm. *Environ Sci Technol.* **2017**, 51(8):4387-4395.
- 581 (52) Coeur-Tourneur, C. C., Cassez, A., and Wenger, J. C.: Rate Coefficients for the Gas-
- Phase Reaction of Hydroxyl Radicals with 2-Methoxyphenol (Guaiacol) and Related
- 583 Compounds, J. Phys. Chem. A, **2010**, 114, 11645–11650.
- 584 (53) Ervens, B., Wang, Y., Eagar, J., Leaitch, W. R., Macdonald, A. M., Valsaraj, K. T., and
- Herckes, P.: Dissolved organic carbon (DOC) and select aldehydes in cloud and fog water:
- the role of the aqueous phase in impacting trace gas budgets, Atmos. Chem. Phys. 2013, 13,
- 587 5117-5135.
- 588 (54) Lanz, V. A., Alfarra, M. R., Baltensperger, U., Buchmann, B., Hueglin, C., and Pr'evot,
- A. S. H.: Source apportionment of submicron organic aerosols at an urban site by factor
- analytical modelling of aerosol mass spectra, Atmos. Chem. Phys. 2007, 7, 1503–1522.
- 591 (55) Craven, J. S., Yee, L. D., Ng, N. L., Canagaratna, M. R., Loza, C. L., Schilling, K. A.,
- 592 ... Seinfeld, J. H. Analysis of secondary organic aerosol formation and aging using positive
- matrix factorization of high-resolution aerosol mass spectra: application to the dodecane low-
- 594 NOx system. Atmos. Chem. Phys. 2012, 12(24), 11795–11817.
- 595 (56) Song, G; Nga L. Ng; Melita Keywood; Varuntida Varutbangkul; Roya
- 596 Bahreini; Athanasios Nenes; Jiwen He; Kee Y. Yoo; J. L. Beauchamp; Robert P.
- 597 Hodyss; Richard C. Flagan and John H. Seinfeld. Particle Phase Acidity and Oligomer
- Formation in Secondary Organic Aerosol, *Environ. Sci. Technol.* **2004**.38 (24), 6582-6589.
- 599 (57) Tolocka, M. P.; Jang, M.; Ginter, J. M.; Cox, F. J.; Kamens, R. M.; Johnston, M. V.
- 600 Formation of Oligomers in Secondary Organic Aerosol. Environ. Sci. Technol. 2004. 38(5),
- 601 1428-1434.

- 602 (58) Li, Y. J.; Yeung, J. W;T., Leung; T. P. I.; Lau, A. P. S.; Chan, C. K. Characterization of
- 603 Organic Particles from Incense Burning Using an Aerodyne High-Resolution Time-of-Flight
- 604 Aerosol Mass Spectrometer. Aero. Sci. Tech. 2012. 46(6), 654–665.
- 605 (59) McLafferty, F. W.; Tureček, F. (2n.d.). Interpretation of mass spectra. 1993.
- 606 (60) Kobayashi, S.; Higashimura, H. Oxidative polymerization of phenols revisited. *Progress*
- 607 in Poly. Sci. **2003**. 28(6), 1015–1048.
- 608 (61) Kawamura, K.; Bikkina, S. A review of dicarboxylic acids and related compounds in
- atmospheric aerosols: Molecular distributions, sources and transformation. Atmos. Res. 2016.
- 610 170, 140–160.
- 611 (62) Anastasio, C.; Faust, B. C.; Rao, C. J. Aromatic carbonyl compounds as aqueous-phase
- photochemical sources of hydrogen peroxide in acidic sulfate aerosols, fogs, and clouds. 1.
- Non- phenolic methoxybenzaldehydes and methoxyacetophenones with reductants (phenols).
- 614 Environ. Sci. Technol. 1997. 31(1), 218–232.

- Figure 1. Overview of photodegradation of SyrAld or ActSyr in ammonium sulfate (AS) or
- ammonium nitrate (AN) solutions: (a) and (b), apparent first-order decays of precursors; (c)
- and (d), aqSOA mass yields. Structures of SyrAld and ActSyr are shown at the bottom of the
- 620 figure
- Figure 2. Three-factor solutions for the PMF analyses of aqSOA in a) and b) SyrAld\_AS; c)
- and d) ActSyr AS; e) and f) SyrAld AN; g) and h) ActSyr AN. Starting concentrations of
- 623 SyrAld and ActSyr were 18.22 and 19.62 mg L<sup>-1</sup> in the AS experiments, respectively, and
- 5.47 and 5.89 mg L<sup>-1</sup> in the AN experiments, respectively.
- Figure 3. (a) and (b), the decay of AMS-detected precursor ions and HPLC-measured
- precursor compounds in SyrAld AS and ActSyr AS, respectively; (c) and (d), time series of
- 627 AMS-detected organic ions that are highly correlated with Factors 1 and 3, respectively, in
- 628 SyrAld AS.
- 629 Figure 4. Van Krevelen diagrams of elemental ratios estimated from PIKA analysis in (a)
- 630 SyrAld\_AS and (b) ActSyr\_AS experiments. Elemental ratios for the first 15 min of reactions
- are not included since the aqSOA concentrations were low, making the elemental ratios
- highly uncertain. Open triangles and circles on the triangle plot are for the reaction time of

- 633 0.25 2 h; filled triangles and squares are for the reaction time of 2 22 h. The arrows
- indicating the direction of change over time are used to guide the eyes.
- 635 Figure 5. Concentrations of oxalic and malic acids detected by IC in offline samples at
- different time of reactions: (a) SyrAld and (b) ActSyr. To compare different experiments, the
- absolute concentrations of the acids are normalized by the concentrations of initial precursor
- 638 compounds.
- 639 Scheme 1. Possible products produced during photooxidation of phenolic carbonyls and the
- 640 formation of oligomeric compounds.

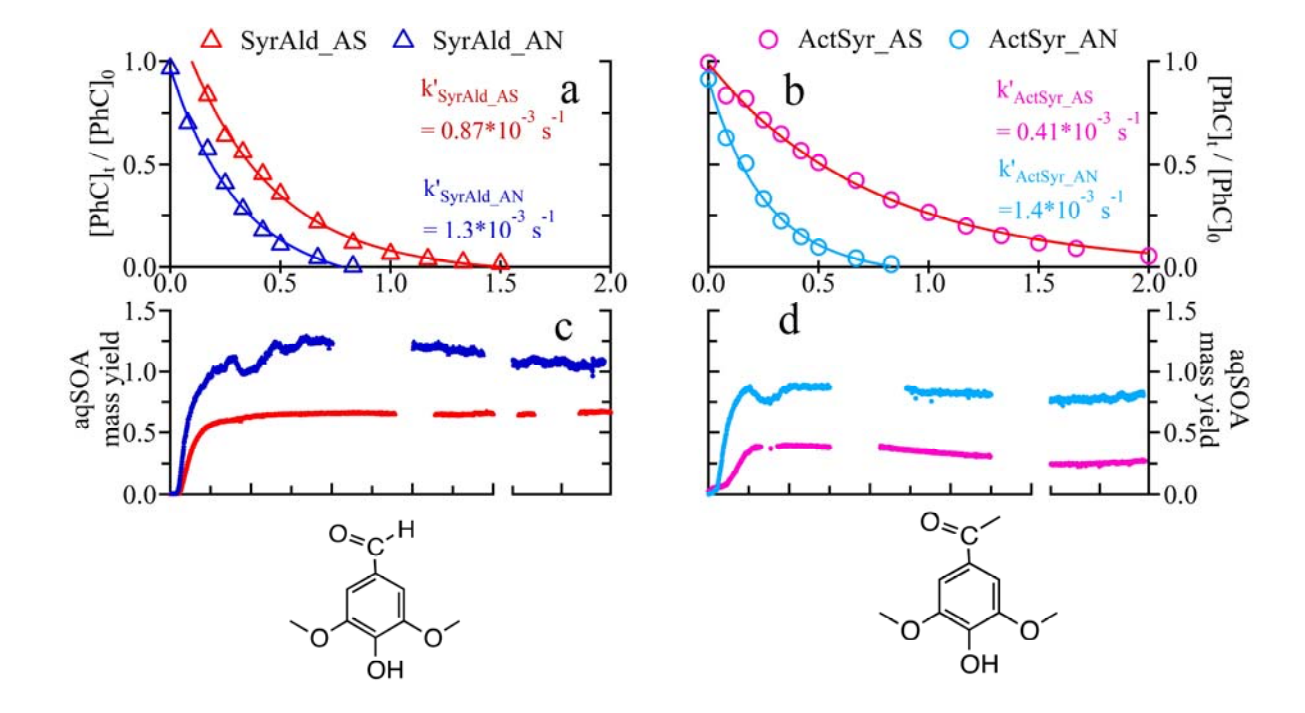
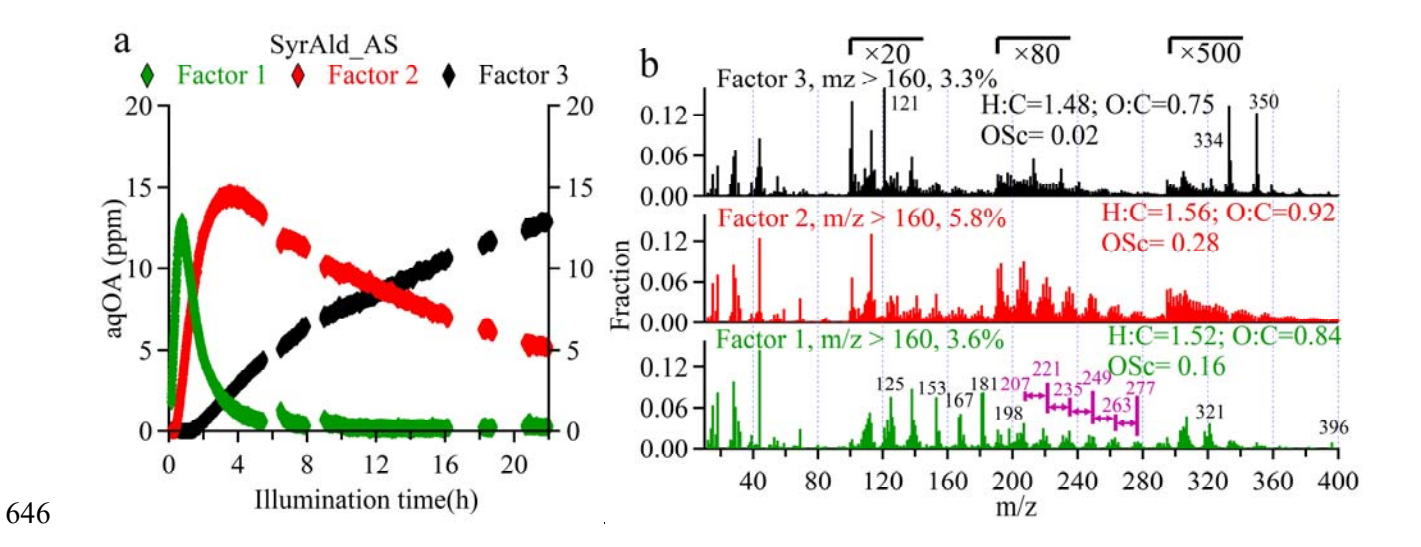


Figure 1. Overview of photodegradation of SyrAld or ActSyr in ammonium sulfate (AS) or ammonium nitrate (AN) solutions: (a) and (b), apparent first-order decays of precursors; (c) and (d), aqSOA mass yields. Structures of SyrAld and ActSyr are shown at the bottom of the figure.



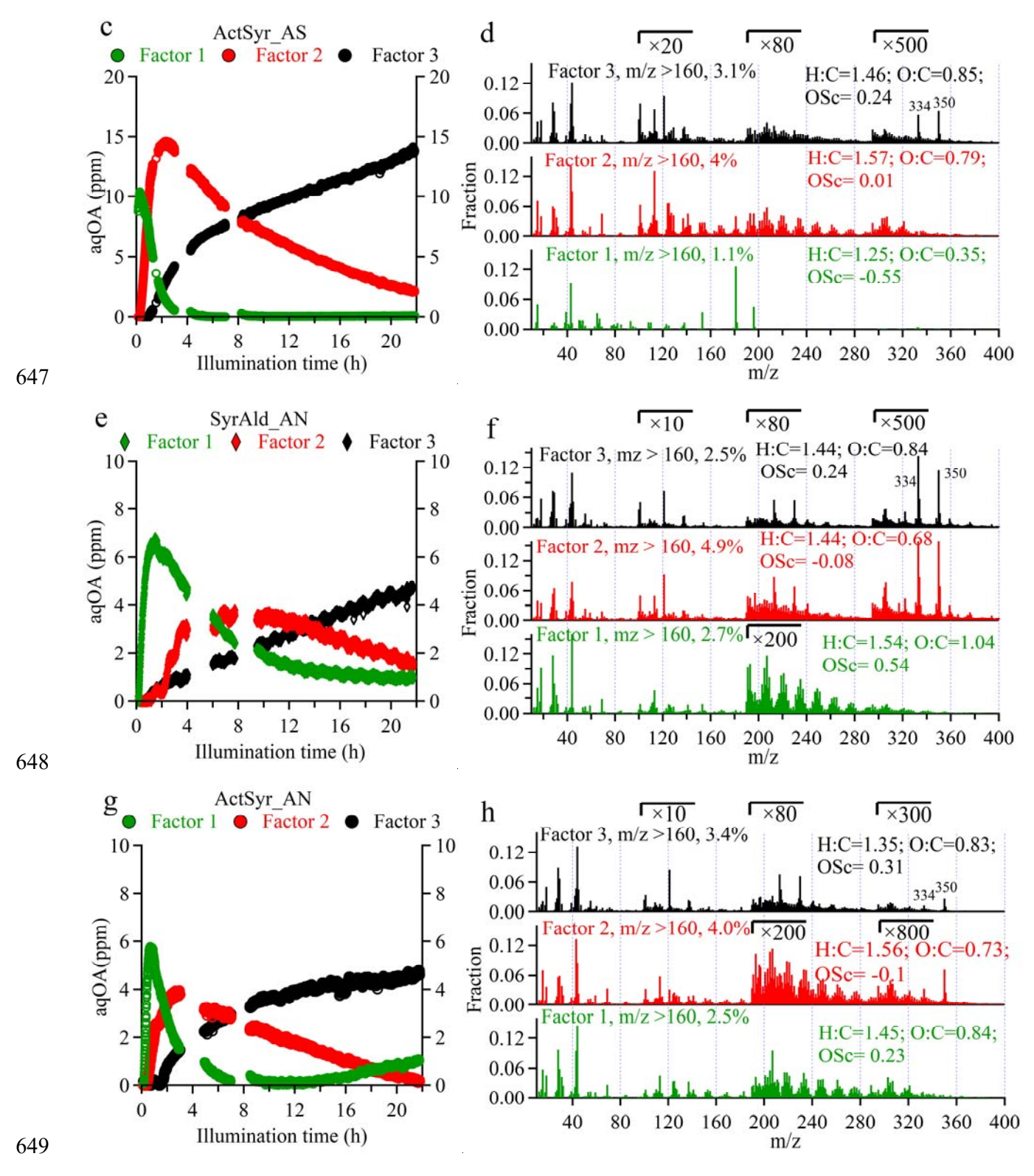


Figure 2. Three-factor solutions for the PMF analyses of aqSOA in a) and b) SyrAld\_AS; c) and d) ActSyr\_AS; e) and f) SyrAld\_AN; g) and h) ActSyr\_AN. Starting concentrations of SyrAld and ActSyr were 18.22 and 19.62 mg L<sup>-1</sup> in the AS experiments, respectively, and 5.47 and 5.89 mg L<sup>-1</sup> in the AN experiments, respectively.

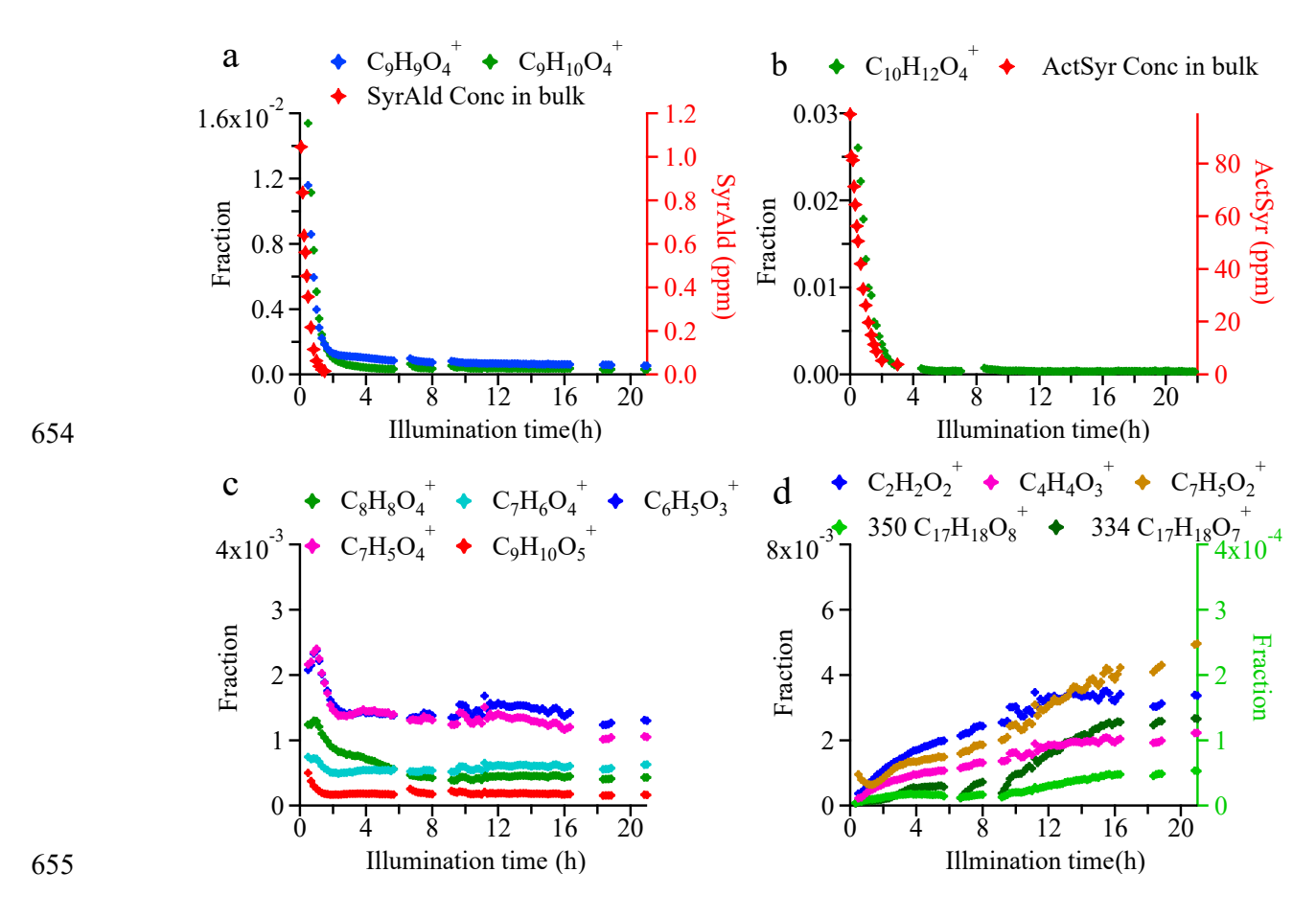


Figure 3. (a) and (b), the decay of AMS-detected precursor ions and HPLC-measured precursor compounds in SyrAld\_AS and ActSyr\_AS, respectively; (c) and (d), time series of AMS-detected organic ions that are highly correlated with Factors 1 and 3, respectively, in SyrAld\_AS.

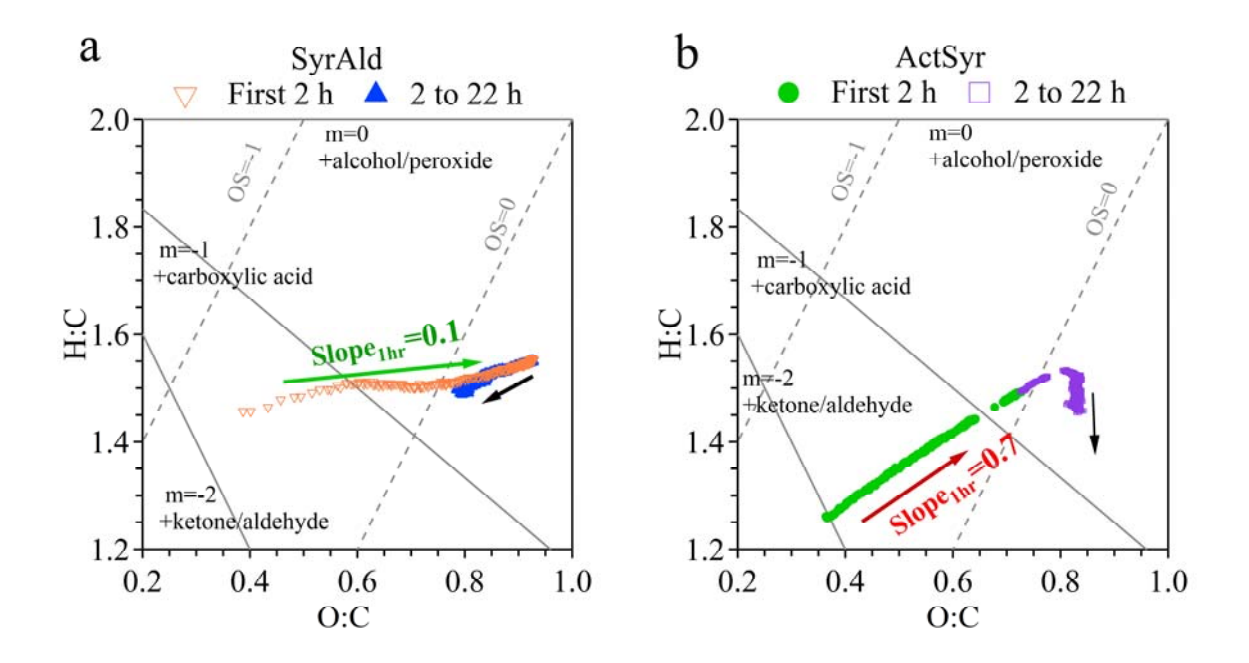


Figure 4. Van Krevelen diagrams of elemental ratios estimated from PIKA analysis in (a) SyrAld\_AS and (b) ActSyr\_AS experiments. Elemental ratios for the first 15 min of reactions are not included since the aqSOA concentrations were low, making the elemental ratios highly uncertain. Open triangles and circles on the triangle plot are for the reaction time of 0.25 - 2 h; filled triangles and squares are for the reaction time of 2 - 22 h. The arrows indicating the direction of change over time are used to guide the eyes.

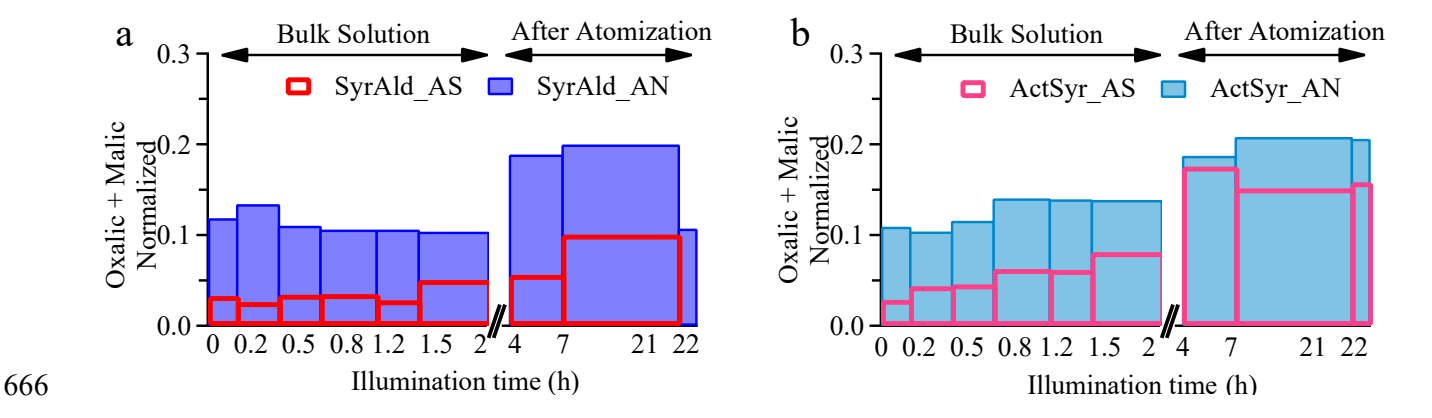
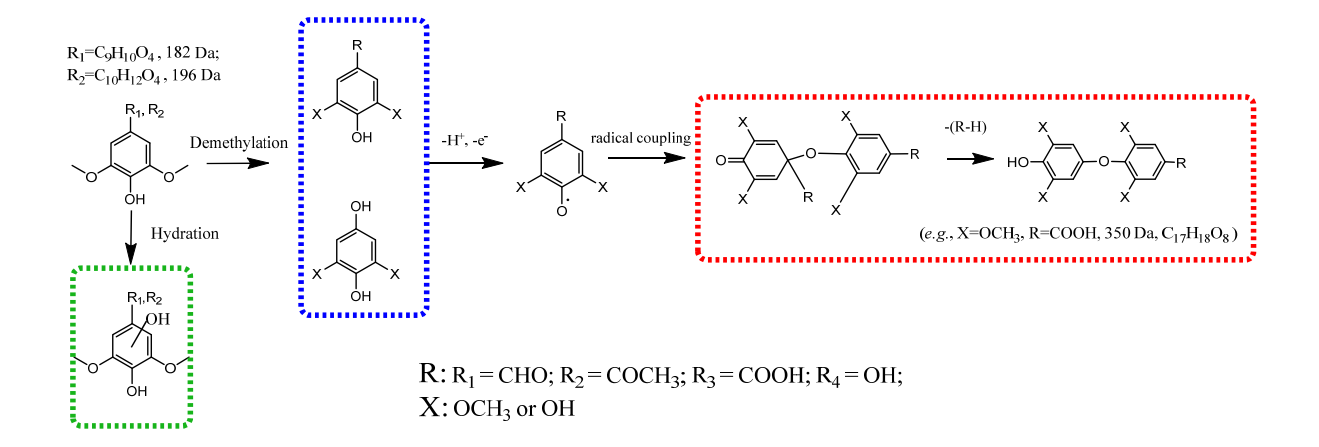


Figure 5. Concentrations of oxalic and malic acids detected by IC in offline samples at different time of reactions: (a) SyrAld and (b) ActSyr. To compare different experiments, the absolute concentrations of the acids are normalized by the concentrations of initial precursor compounds.



Scheme 1. Possible products produced during photooxidation of phenolic carbonyls and the formation of oligomeric compounds.

# **Supporting Information**

Formation and evolution of aqSOA from aqueous-phase reactions of phenolic carbonyls: comparison between ammonium sulfate and ammonium nitrate solutions

Dan Dan Huang<sup>1</sup>, Qi Zhang<sup>2,\*</sup>, Heidi H.Y. Cheung<sup>3</sup>, Lu Yu<sup>2</sup>, Shan Zhou<sup>2</sup>, Cort Anastasio<sup>4</sup>, Jeremy D. Smith<sup>4</sup>, Chak K. Chan<sup>1,\*</sup>

<sup>1</sup> School of Energy and Environment, City University of Hong Kong, Hong Kong, China

<sup>2</sup> Department of Environmental Toxicology, University of California, 1 Shields Ave. Davis, CA 95616, USA

<sup>3</sup> Division of Environment, Hong Kong of University of Science and Technology, Hong Kong, China

<sup>4</sup> Department of Land, Air and Water Resources, University of California, 1 Shields Ave, Davis, CA 95616, USA

\*Corresponding authors:

Qi Zhang, dkwzhang@ucdavis.edu; Phone: 530-752-5779 (Office); Fax: 530-752-3394

Chak K. Chan, Chak.K.Chan@cityu.edu.hk; Phone: 852 - 3442-5593; Fax: 852-3442-0688

This supplementary document contains three appendixes, fifteen figures and one table, 19 pages in total.

# S-1Subtraction of non-OA CO<sub>2</sub><sup>+</sup>

Pieber et al. (2016)<sup>1</sup> suggested that the non-OA CO<sub>2</sub><sup>+</sup> intensities generated in the AMS chamber can be correlated with the intensities of (NO<sup>+</sup> + NO<sub>2</sub><sup>+</sup>) by measuring pure NH<sub>4</sub>NO<sub>3</sub> at different concentrations. However, such measurements were not made in our study and we assumed the ratio of organic CO<sub>2</sub><sup>+</sup> obtained in the dark AN experiments is from the non-OA CO<sub>2</sub><sup>+</sup>, which is a reasonable assumption since concentrations of OA components in the solution are low before the lights are turned on. We found that the NO<sub>2</sub><sup>+</sup> peak is likely interfered by the adjacent organic peak (CH<sub>2</sub>O<sub>2</sub><sup>+</sup>) in the organic spectrum of illuminated experiments. Since non-OA CO<sub>2</sub><sup>+</sup> showed good correlation with NO<sup>+</sup> (Figure S5), the signal intensity of non-OA CO<sub>2</sub><sup>+</sup> is obtained as follows:

$$non - OA CO_{2AN}^+ = 0.07 * NO_{AN}^+$$

After modification of the fragmentation table, the organic mass spectra of "ActSyr\_AS Dark" and "ActSyr\_AN Dark" are comparable to the standard mass spectrum of ActSyr in NIST database as shown in Figure S8, giving us confidence that the data processing and the method that applied to modify the fragmentation table are appropriate. However, the "SyrAld\_AN Dark" is actually quite different from "SyrAld\_AS Dark". We note that the AMS detected organic concentration in SyrAld\_AN Dark (CE=1) was only around 2 μg/m³ but it was around 40 μg/m³ in SyrAld\_AS Dark. The low organic concentration in "SyrAld\_AN Dark" likely results in high uncertainty in the mass spectrum and the elemental ratios in AMS analyses. Differences in the initial concentrations of the precursor compound used in SyrAld\_AN Dark (30μM) and SyrAld\_AS Dark (100μM) as well as the efficiency of the atomizer may contribute to the large differences in organic concentrations in the SyrAld AS Dark and SyrAld\_AN Dark experiments. Hence, it is reasonable to consider that the organic concentration in SyrAld\_AN Dark is too low to generate a reasonable organic mass spectrum. Because of this, the first 15 min of the reactions for all experiments are not included in the mass spectra of PMF and elemental analysessince the aqSOA concentrations are low making the spectra highly uncertain.

## S-2. PMF analysis

The unit mass resolution AMS data were processed with both SQUIRREL 1.57and PIKA V1.16 analysis toolkits. We have utilized the organic data matrices and the corresponding error

matrices from both "SQUIRREL" and "PIKA" for the PMF analyses. m/z ranges of the data from "SQUIRREL" and "PIKA" in PMF analyses are 12 – 450 and 12 - 200, respectively. SQUIRREL analysis is good for the analysis of high-molecular weight ions as it exhibits a more favorable signal to noise ratios; PIKA analysis is good for ion identification and elemental analysis.

The error matrices were pretreated using the PMF Evaluation Toolkit (PET) following the procedure described in *Ulbrich et al.* [2009].<sup>2</sup> Variables with a signal-to-noise (SNR) ratio less than 0.2 ("bad" variables) were removed and variables with SNR ranging between 0.2 and 2 ("weak" variables) were downweighted by a factor of 2. Since O<sup>+</sup>, HO<sup>+</sup>, H<sub>2</sub>O<sup>+</sup> and CO<sup>+</sup> are related proportionally only to  $CO_2^+$  in the fragmentation table, the error values for each of these m/z were multiplied by sqrt (5) to avoid excessive weighting of CO<sub>2</sub><sup>+</sup> as prescribed by Ulbrich et al. [2009].<sup>2</sup> The data were analyzed using the PMF2 algorithm<sup>3</sup> with fpeak varying between -1 and 1. The PMF results are evaluated using the PMF Evaluation Tool in Igor Pro developed by  $[2009]^2$ (PET, Ulbrich al. Version 2.06, http://cires1.colorado.edu/jimenezgroup/wiki/index.php/PMF-AMS Analysis Guide). The PMF solution was carefully evaluated according to the procedures outlined in Zhang et al. (2011).<sup>4</sup>

For each dataset, the optimal solution was determined after examining the residuals of PMF fits. For all four sets of experiments, Q/Qexpected decreased from p=1 to p=3, beyond which the decreases in Q/Qexpected are small. The PMF results for aqSOA formation from all four experiments exhibit three distinct time series with their corresponding factor mass spectral profiles. When the PMF solution is increased to four factors, the addition of one more factor would not enhance the information for the factorization from a residual point of view. Also, adding one more factor will lead to the missing point of FPEAK, which might due to the relatively small data amount for lab experiments compared with the filed data. Splitting more factors from the organic matrices will have more solutions that are not converging. The rotational ambiguity of solutions was examined by changing the parameter FPEAK, and an FPEAK value of 0 was used for all data sets in the PMF analysis on organic mass spectra. The robustness of solutions were evaluated by starting PMF with different initial conditions (parameter SEED, *i.e.*, Figure S14).

Bootstrapping is performed for the current PMF solution to evaluate the statistical

uncertainty of the candidate solution (*i.e.*, Figure S15). We made assessment of the uncertainty of the factors with 100 bootstrapping runs. Black lines in time series (TS) and black sticks in mass spectra (MS) represent the PMF candidate solutions. Overall, the PMF solutions show a similar range in MS and TS to the bootstrapping 1-σ variation bars. The bootstrapping analysis shows our current PMF solution is reasonably robust and appropriate.

#### S-3. aqSOA yields

The added ammonium sulfate or sulfuric acid was used as an internal standard to relate aerosol concentration ( $\mu g \, m^{-3}$ ) measured by AMS to liquid concentration ( $mg \, L^{-1}$ ). Organic to inorganic ratio can be measured online by AMS before and after the reactions starts. The organic concentration at time t in the solution can thus be calculated as follows:

$$\frac{(aqOrg)_t}{aqInorg} = \left(\frac{Org}{Inorg}\right)_{AMS}$$

$$(aqOrg)_t = aqInorg (constant) * \left(\frac{Org}{Inorg}\right)_{AMS}$$

The aqSOA can thus be calculated as:

$$aqSOA = (aqOrg)_{t\_illu\_AMS} - (aqOrg)_{t\_dark\_AMS}$$

where  $(aqOrg)_{t\_dark\_AMS}$  is determined before each experiment starts. And aqSOA yield can subsequently be calculated:

$$Yield = \frac{(aqOrg)_{t\_illu\_AMS} - (aqOrg)_{t\_dark\_AMS}}{ArOH \ reacted \ determined \ by \ HPLC}$$

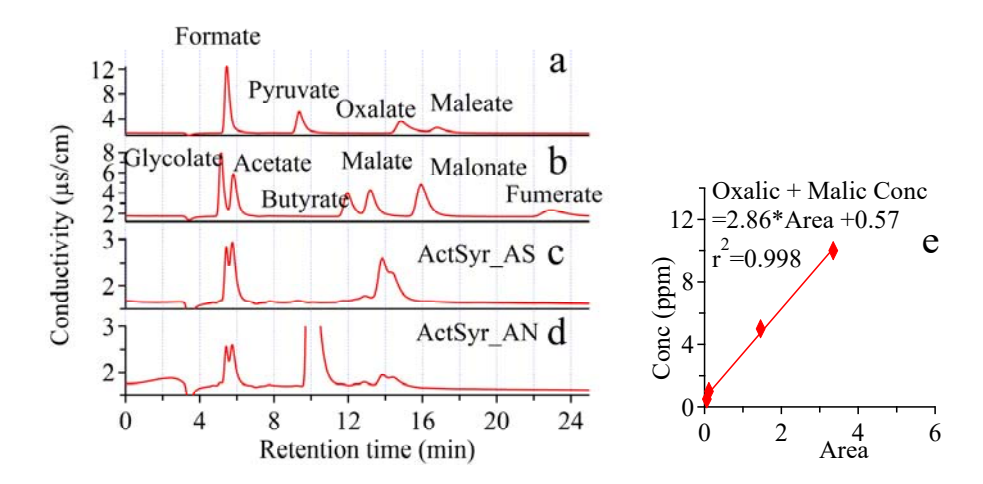


Figure S1. IC chromatographs of a) standard mixture of formic, pyruvic, oxalic, maleic acids; b) standard mixture of acetic, butyric, malic and malonic acids; c) one of the offline samples in ActSyr\_AS; d) one of the offline samples in ActSyr\_AN; e) calibration curve for quantification of oxalic and malic acids. For the same precursor, organic anions in AS experiment were eluted at similar retention time as the AN one, *i.e.*, the lumped peaks at t = 6min and t = 14min in Figures S1c and S1d, indicating the presence of the same organic species in AS and AN experiments. Other organic anions might as well present in the reaction solutions, but they are below the detection limit using the current chromatographic method and hence are not included in the current discussions.

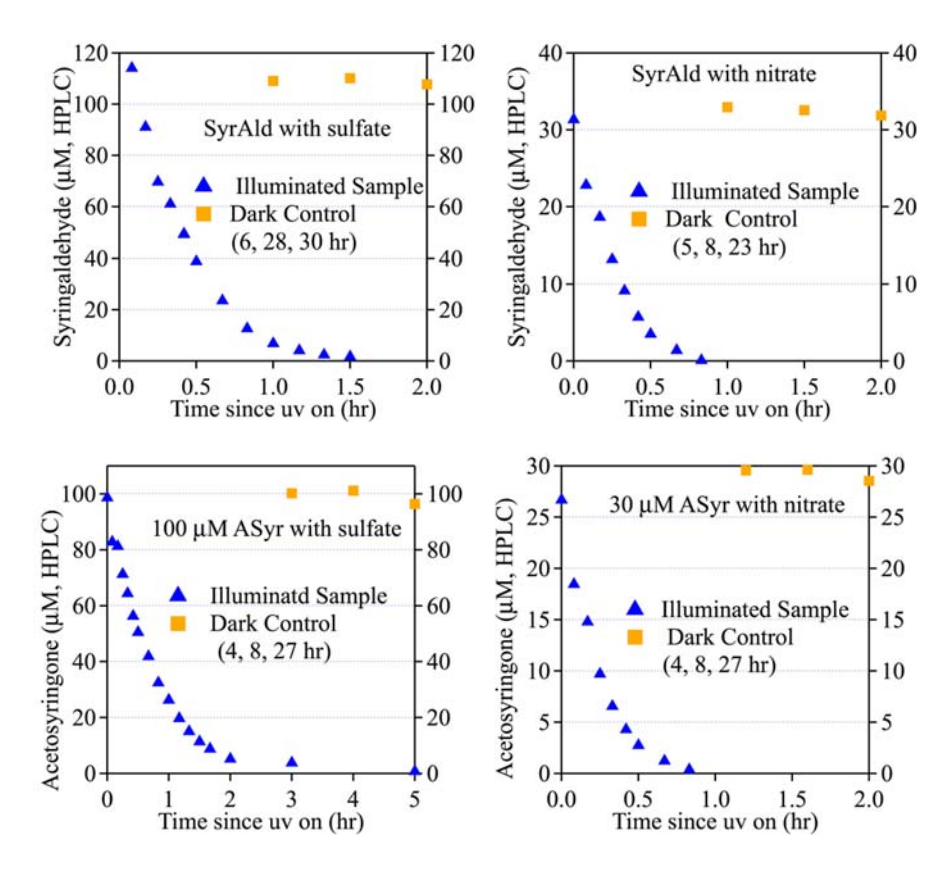


Figure S2 Precursor decay as measured by HPLC in illuminated and dark samples

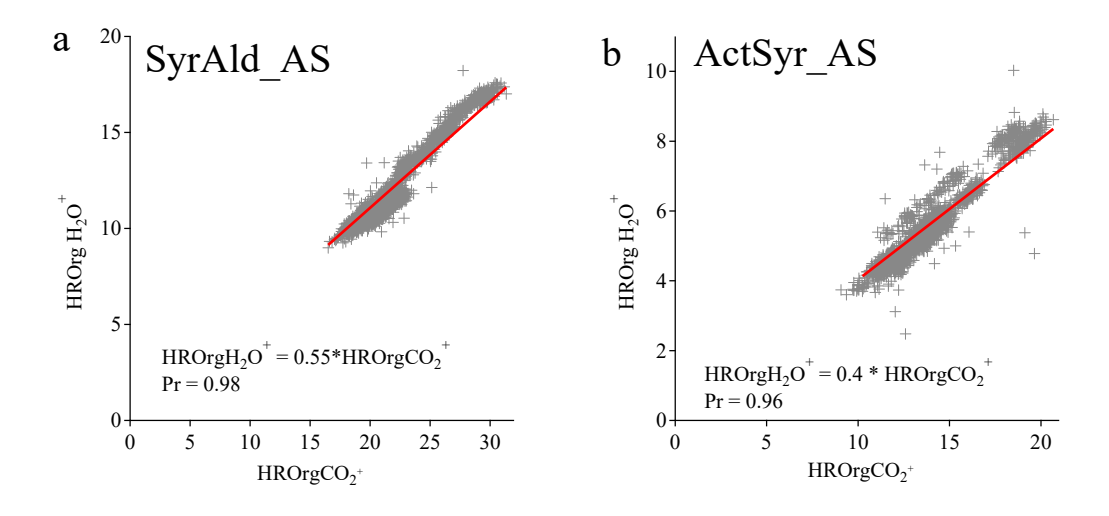


Figure S3. Correlation of Organic H<sub>2</sub>O<sup>+</sup> vs. Organic CO<sub>2</sub><sup>+</sup> in a) SyrAld and b) ActSyr experiments.

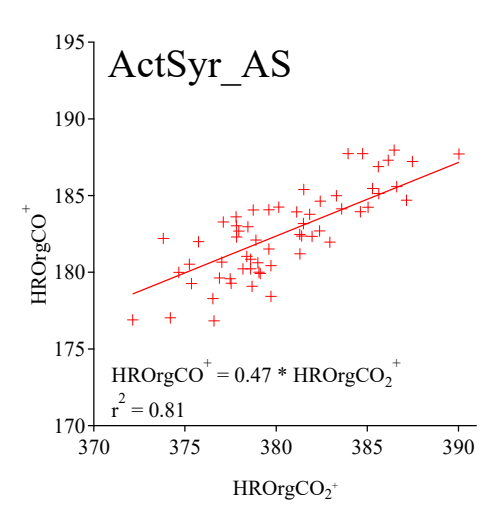


Figure S4. Correlation of Organic CO<sup>+</sup> vs. Organic CO<sub>2</sub><sup>+</sup> in ActSyr AS

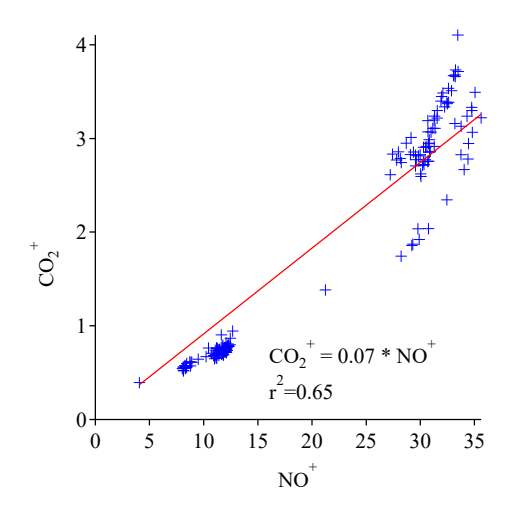
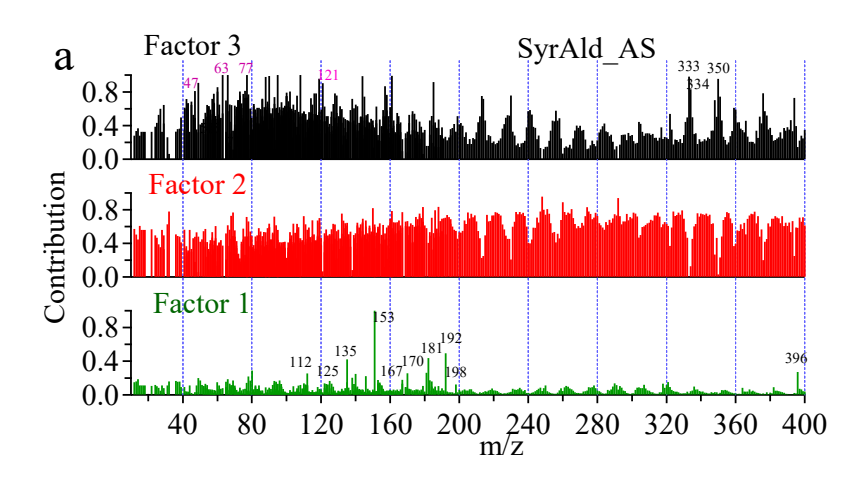
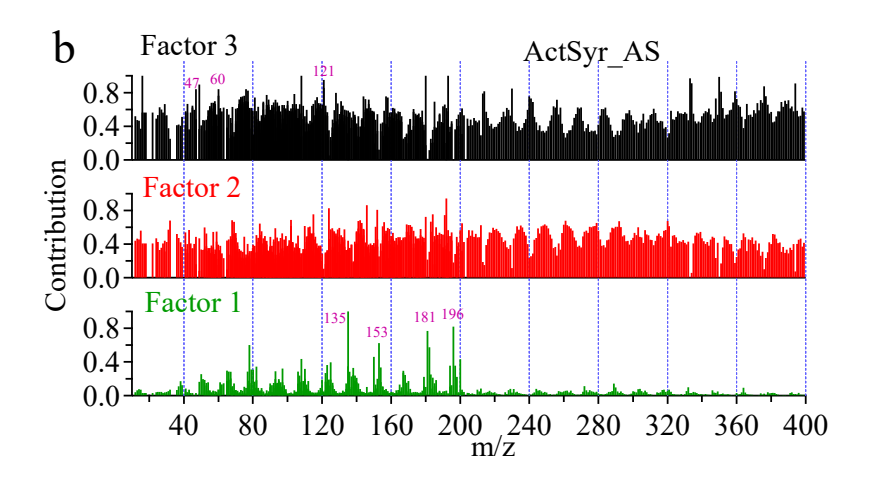
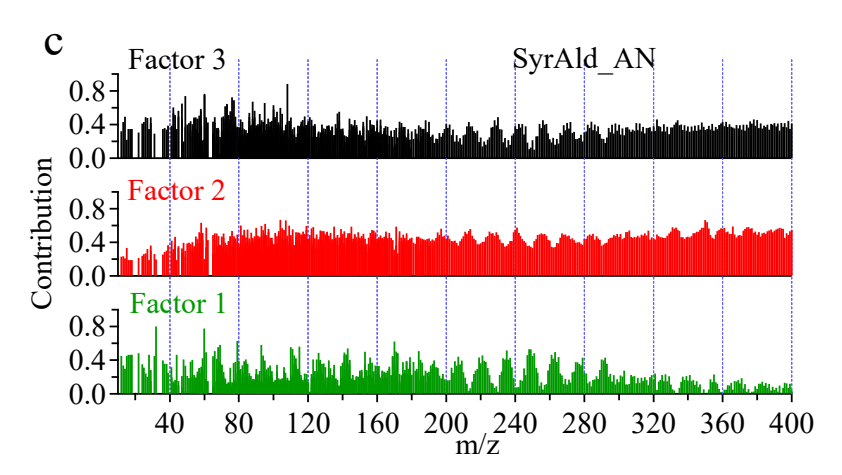


Figure S5. Correlation of non-OA CO2<sup>+</sup> vs. NO<sup>+</sup>







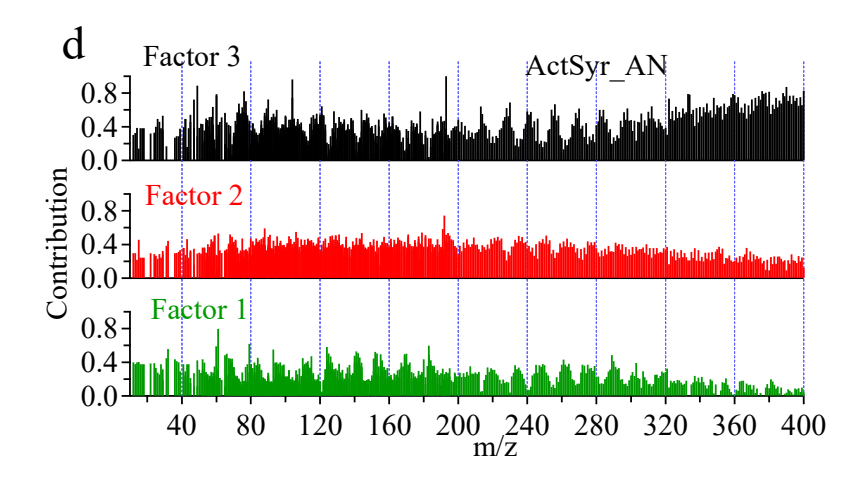


Figure S6. Contribution of each factor to each m/z for: a) SyrAld\_AS; b) ActSyr\_AS; c) SyrAld\_AN; d) ActSyr\_AN.

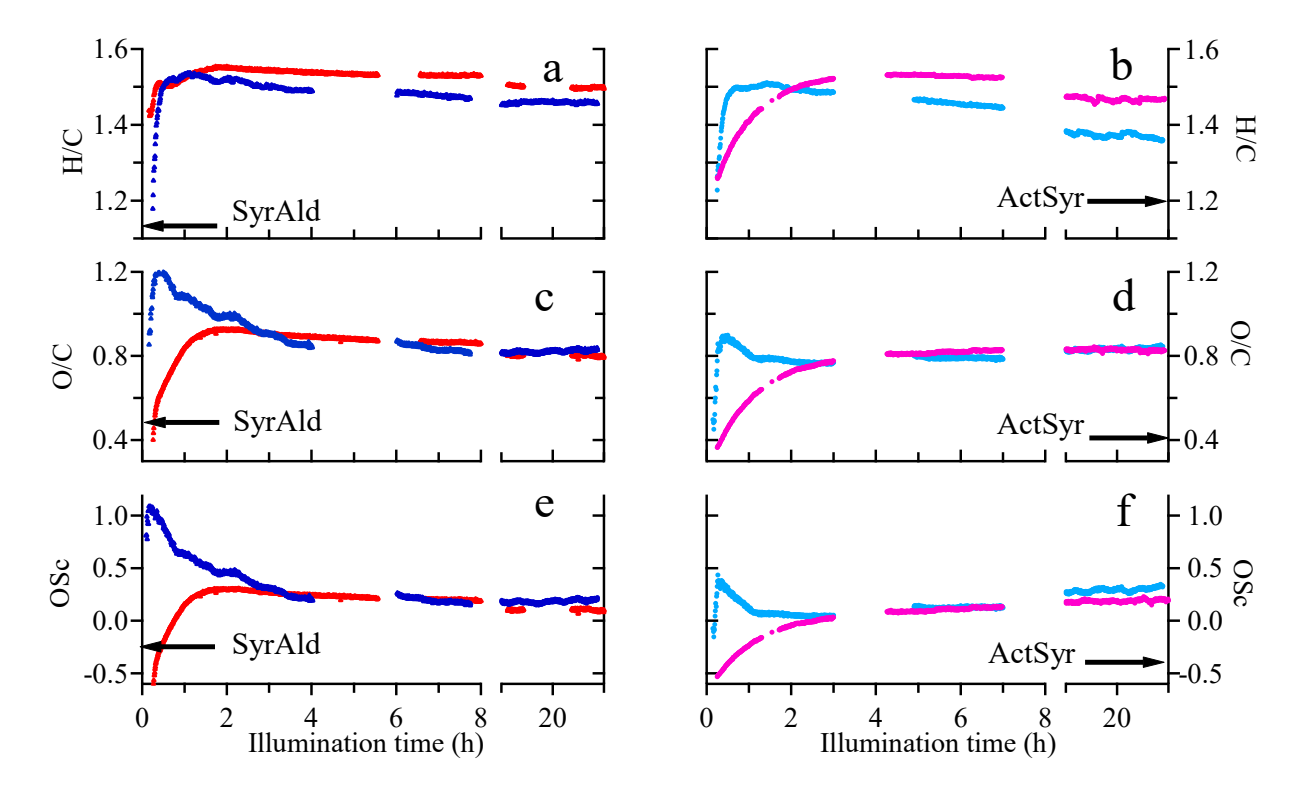


Figure S7 Photodegradation of SyrAld or ActSyr in ammonium sulfate (AS) or ammonium nitrate (AN) solutions: (a) - (d), elemental ratios of aqSOA; (e) - (f) average carbon oxidation states (OS<sub>C</sub>) of aqSOA.

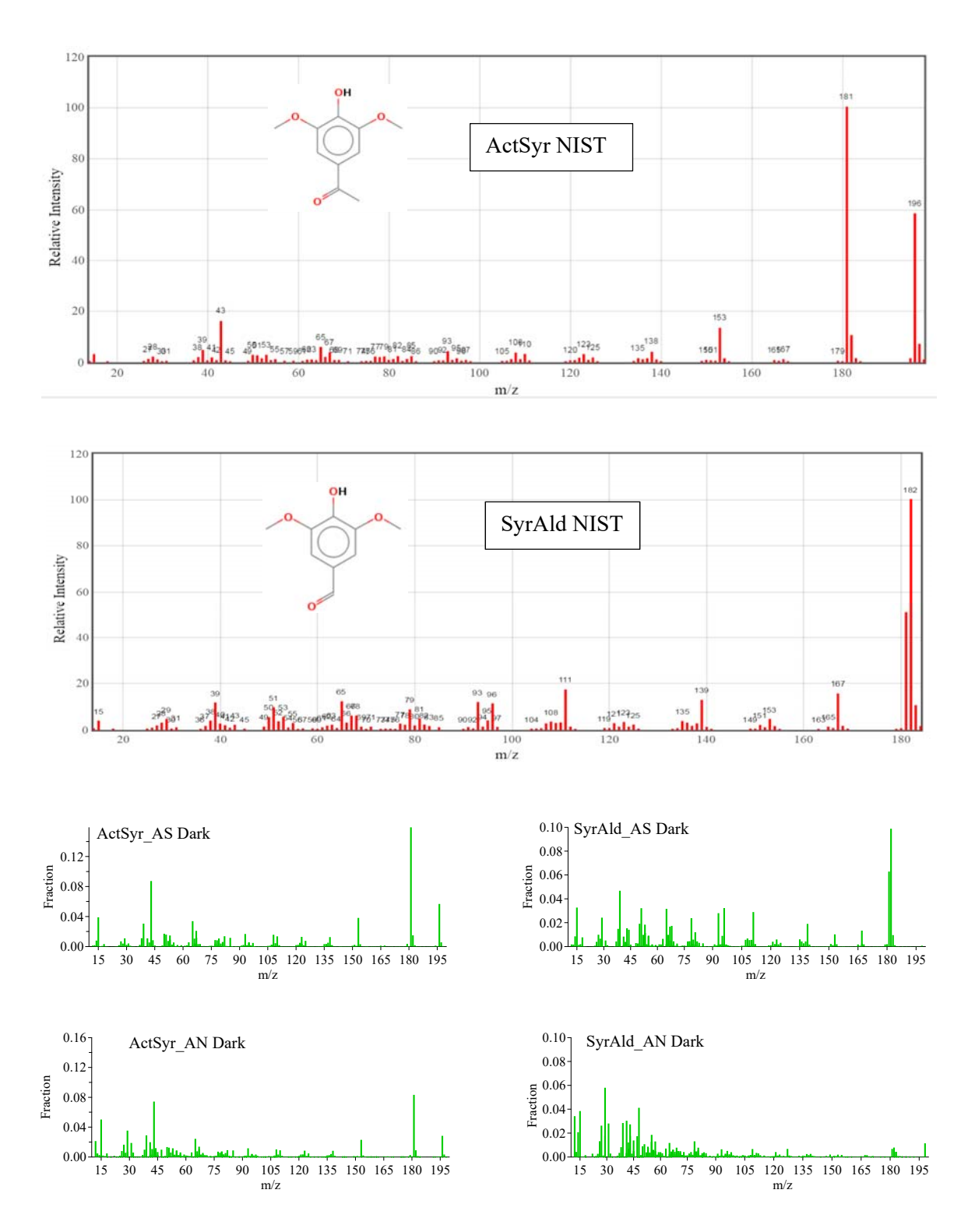


Figure S8. NIST and AMS organic mass spectra of each pure precursor compound mixed with different inorganic salts before illumination.

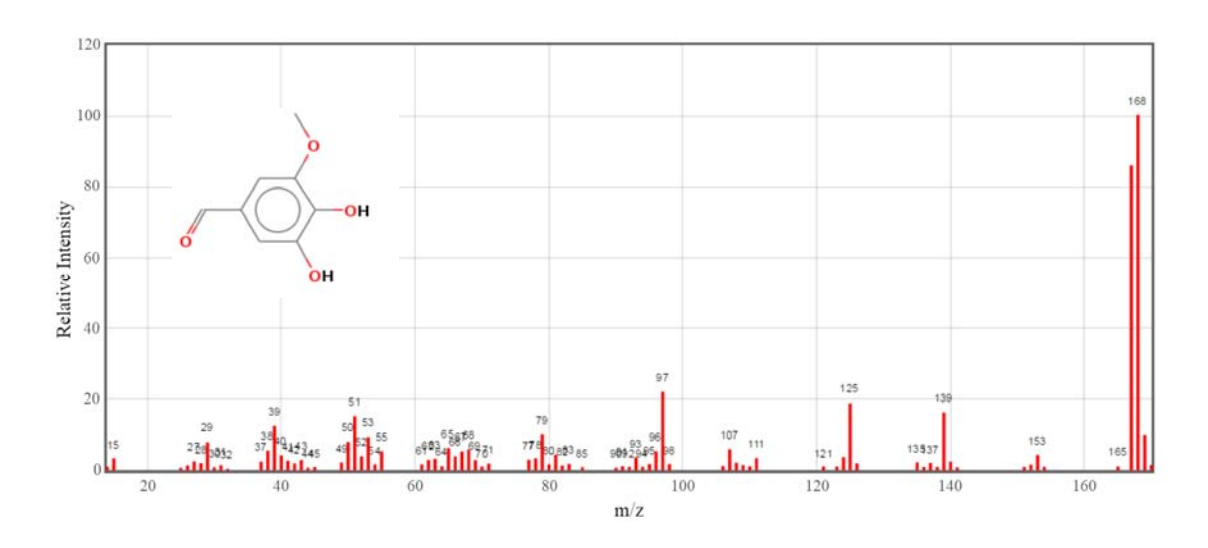


Figure S9. NIST mass spectrum of 3, 4- Dihydroxy-5-methoxybenzaldehyde,  $C_8H_8O_4$  (MW = 168).

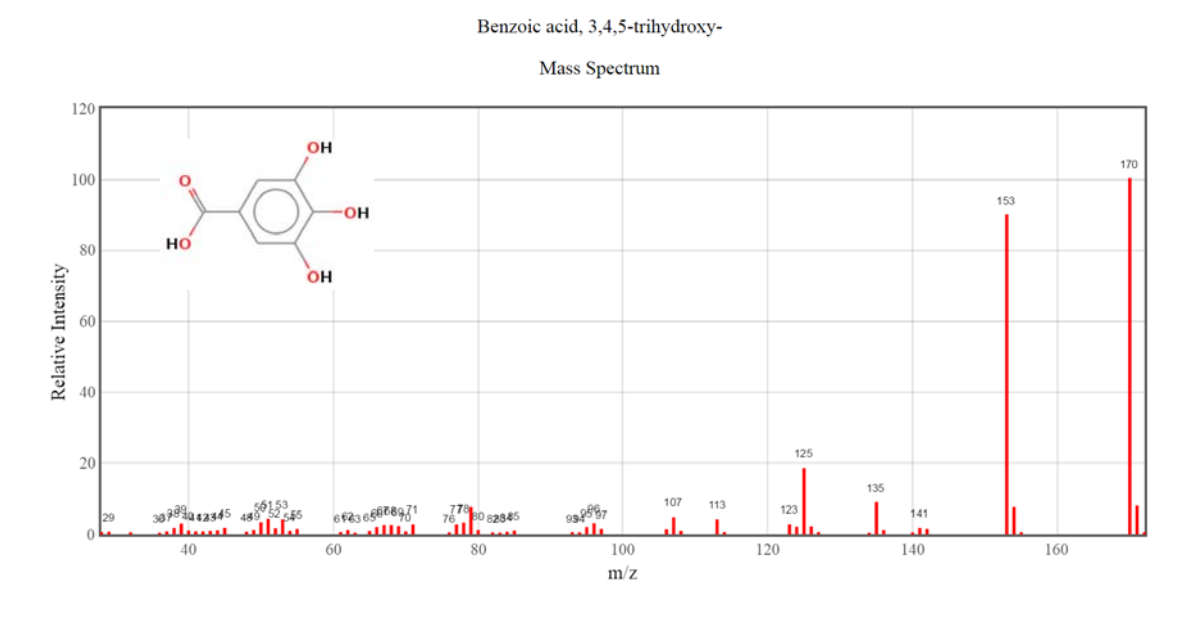


Figure S10. NIST mass spectrum of 3,4,5-Trihydroxybenzoic acid, C<sub>7</sub>H<sub>6</sub>O<sub>5</sub> (MW = 170).

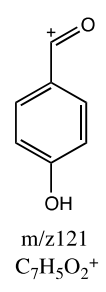


Figure S11. Proposed structure for fragment m/z 121

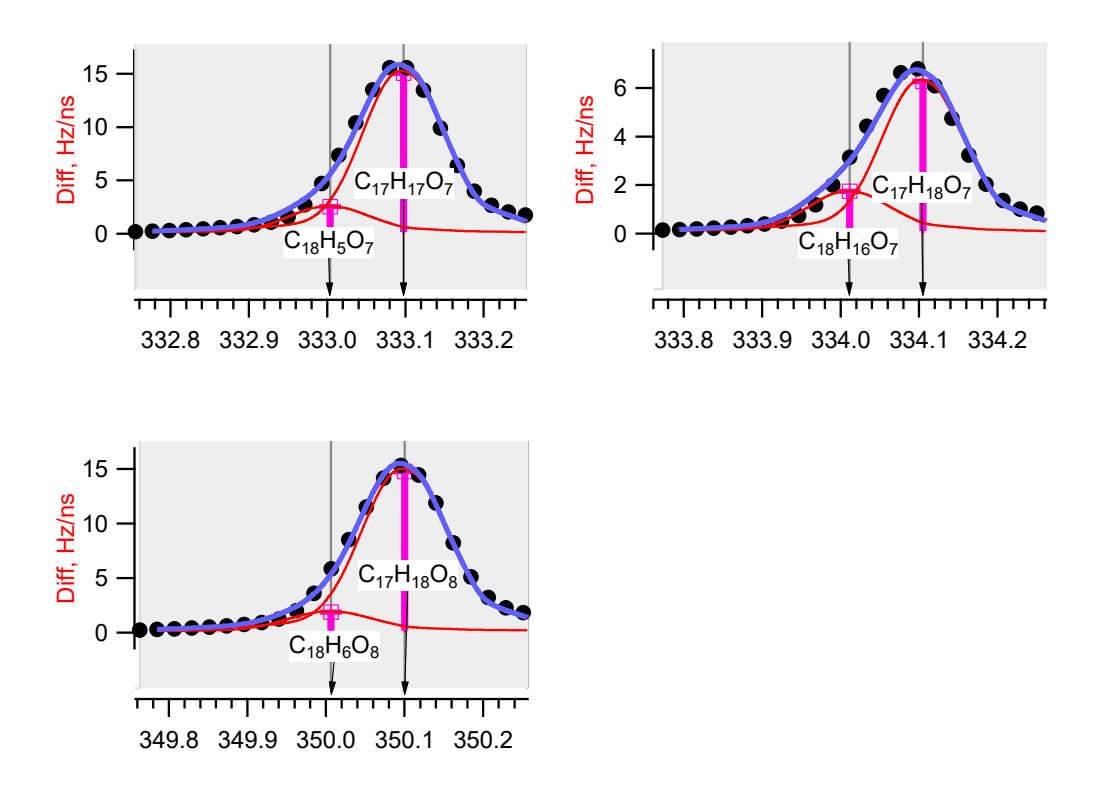
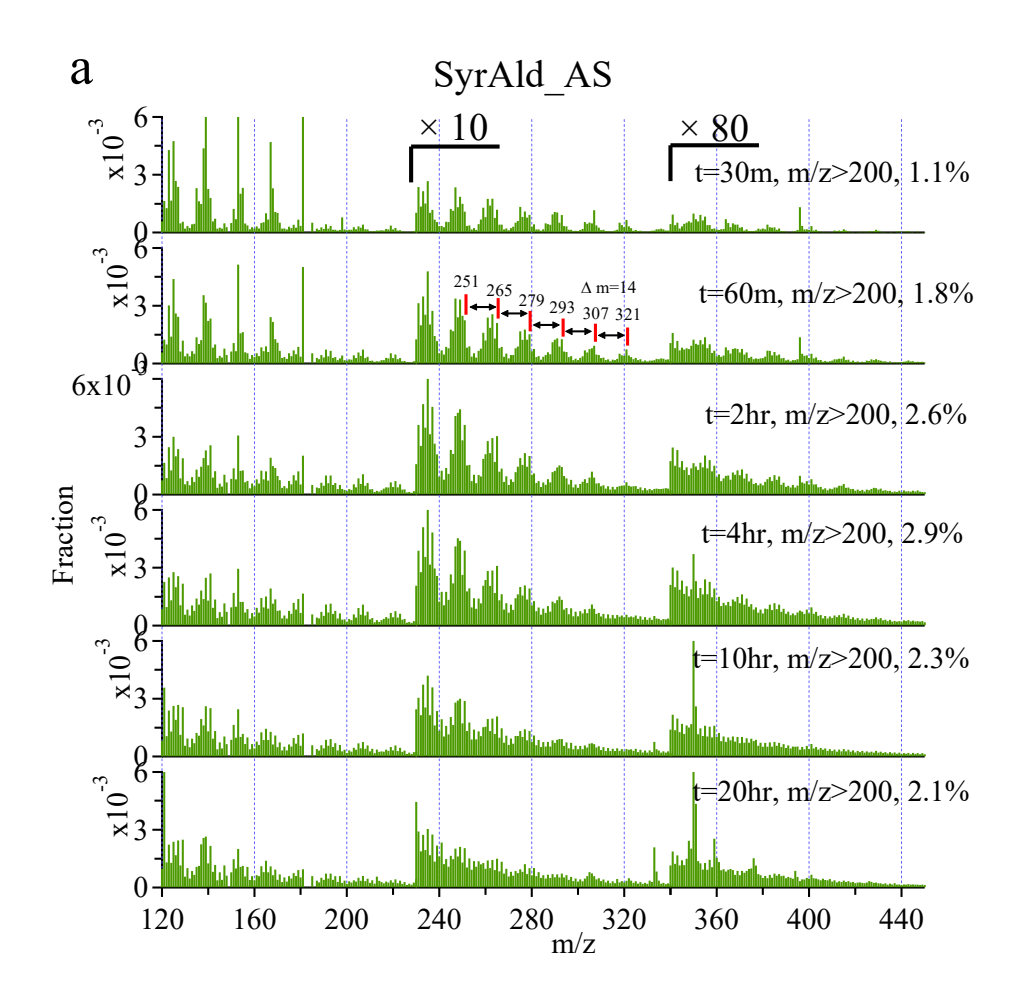
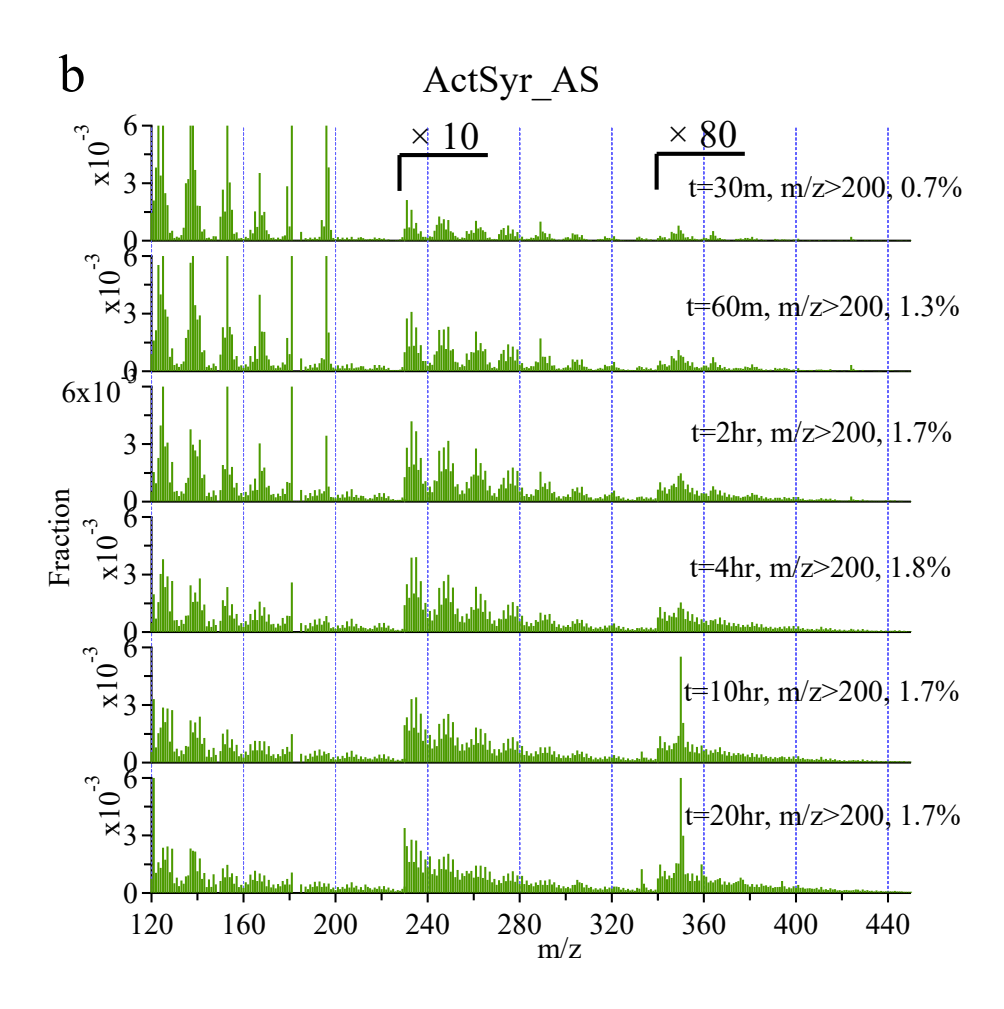
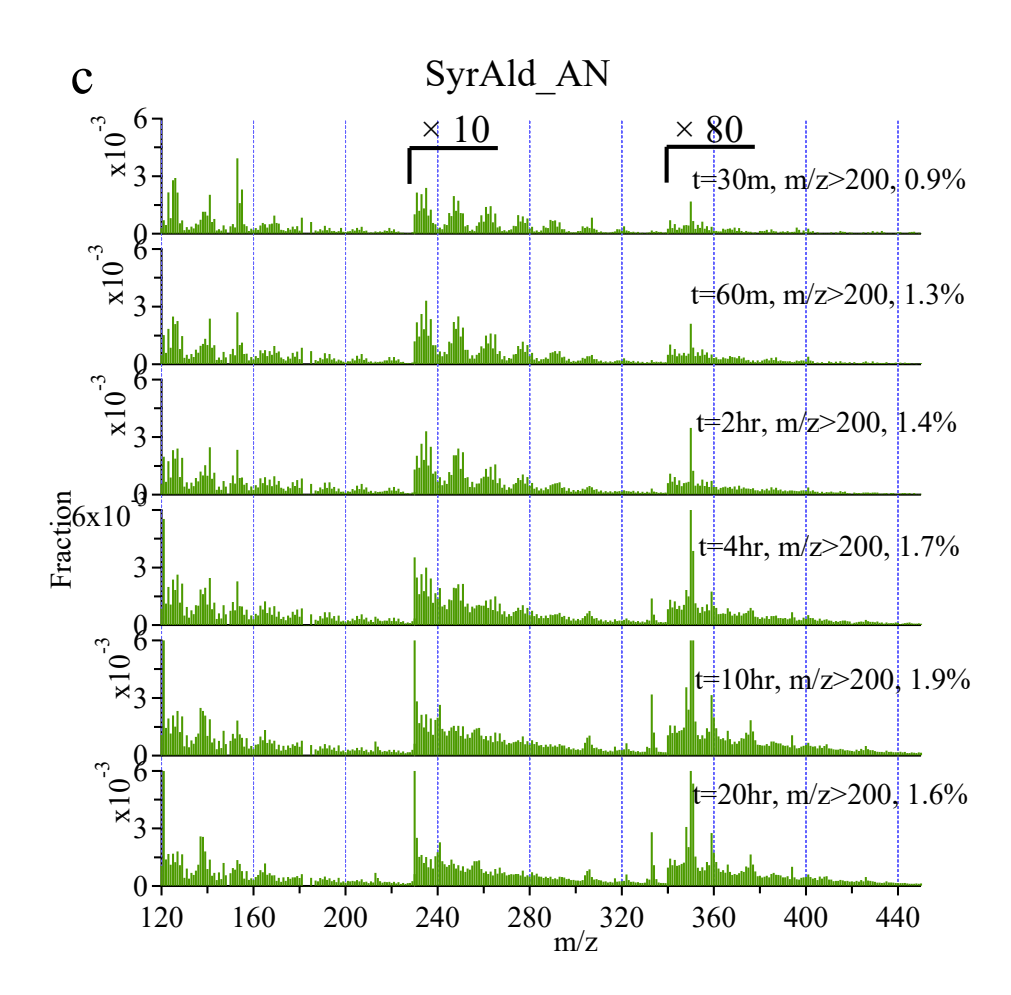


Figure S12. Peak fittings for the dimer compounds







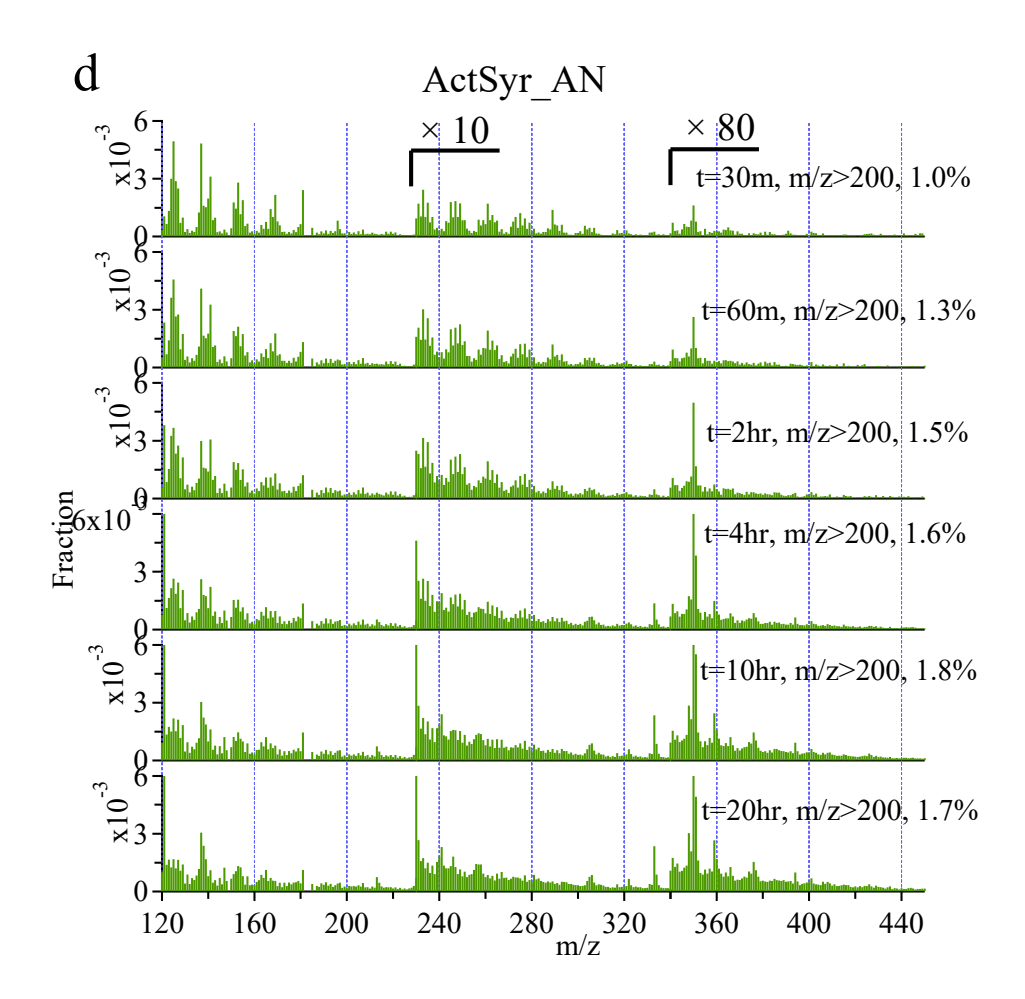


Figure S13. Mass spectra of aqSOA at different time of reactions in (a) SyrAld\_AS, (b) ActSyr\_AS, (c) SyrAld\_AN, and (d) ActSyr\_AN experiments.

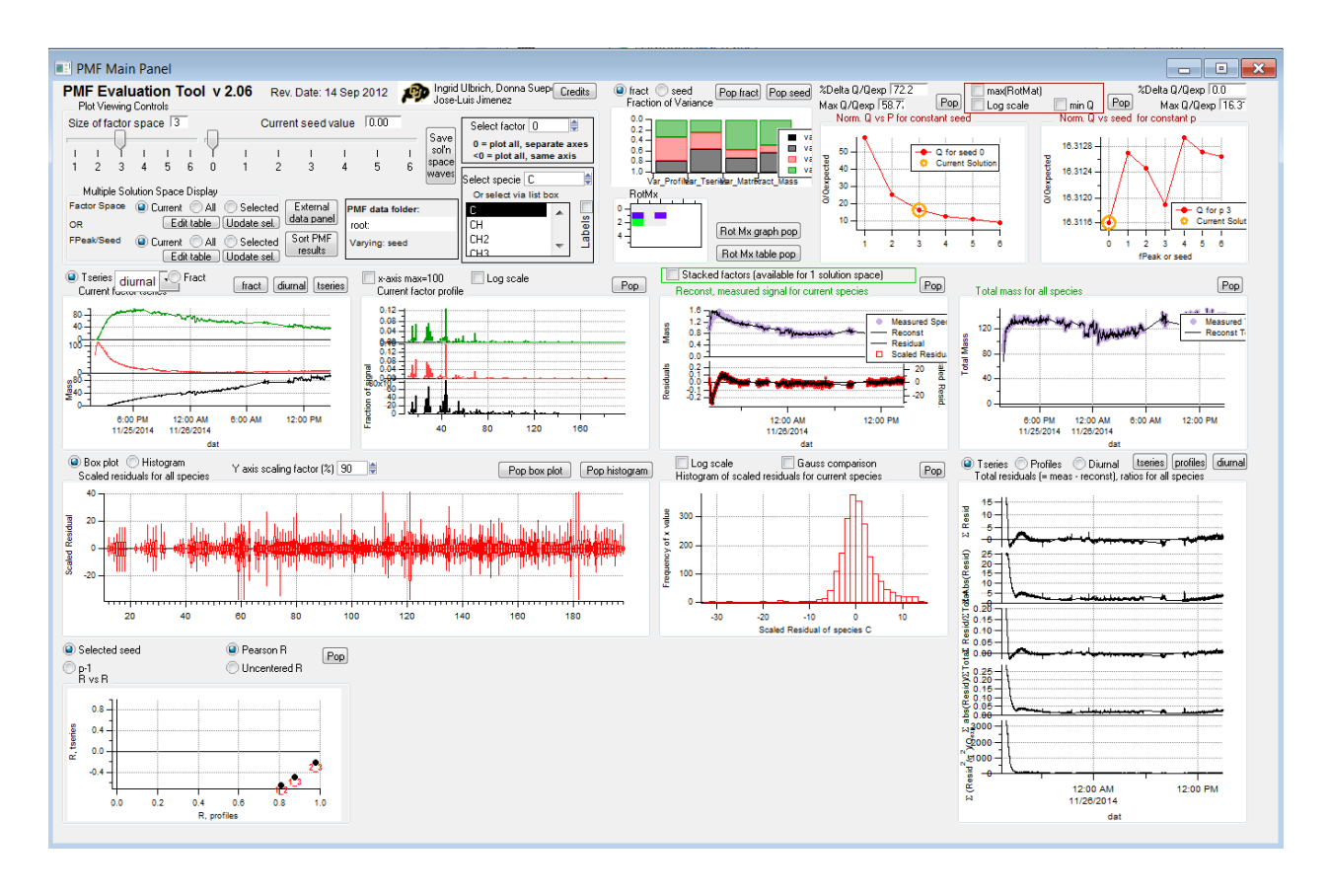


Figure S14Three-factor solution for PMF analysis of SyrAld\_AS, Diagnostic plot, fPeak=0, Seed varies from 0 to 6

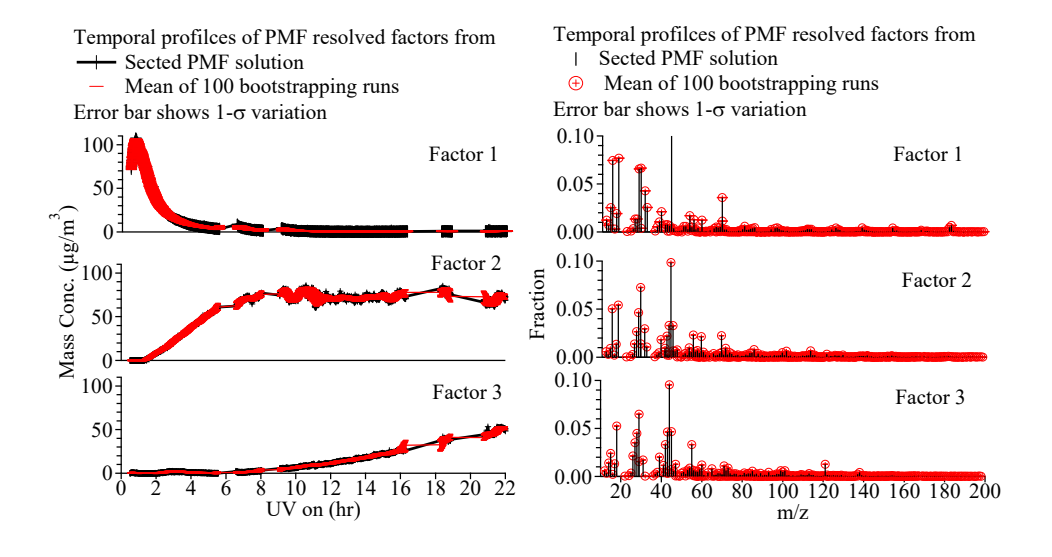


Figure S15 Bootstrapping analysis for the three-factor solution for SyrAld AS

Precursor information Chemical structure Chemical formula O/C, H/C, OSc	Syringaldehyde		Acetosyringone	
	(SyrAld)		(ActSyr)	
	0 H		О СН3	
	H <sub>5</sub> CO OCH <sub>3</sub>		н,со он	
	C <sub>9</sub> H <sub>10</sub> O <sub>4</sub> M.W. 182		C <sub>10</sub> H <sub>12</sub> O <sub>4</sub> M.W. 196	
	0.44,1.11,-0.23		0.4,1.2,-0.4	
Inorganic components and initial concentrations	NH4NO3 (AN) 200 μM	(NH4)2SO4 (AS) 22.7μM	NH4NO3 (AN) 200 μM	(NH <sub>4</sub> ) <sub>2</sub> SO <sub>4</sub> (AS) 22.7μΜ
Initial concentrations of organic	30 μM (5.47ppm)	100 μM (18.22ppm)	30 μM (5.89ppm)	100 μM (19.62ppm)
Apparent first order decay rate (s <sup>-1</sup> )	1.3×10 <sup>-3</sup>	0.87×10 <sup>-3</sup>	1.4×10 <sup>-3</sup>	0.41×10 <sup>-3</sup>
TOC (ppm) when all precursors were consumed	3.3	9.2	3.5	11
OM/OC when all precursors were consumed	2.4	2.3	2.1	2.1
aqSOA(ppm) yield when all precursors were consumed	0.9	0.6	0.8	0.4
O/C,H/C,OSc when all precursors were consumed	1.1, 1.52, 0.68	0.91, 1.54, 0.28	0.83, 1.49, 0.17	0.68, 1.46,

Table S1 Information for different experiments

## **References:**

- (1) Pieber, S. M.; El Haddad, I.; Slowik, J. G.; Canagaratna, M. R.; Jayne, J. T.; Platt, S. M.; Prévôt, A. S. H. Inorganic Salt Interference on CO <sub>2</sub> <sup>+</sup> in Aerodyne AMS and ACSM Organic Aerosol Composition Studies. *Environ. Sci. Technol.* **2016**. 50(19), 10494–10503.
- (2) Ulbrich, I. M.; Canagaratna, M. R.; Zhang, Q.; Worsnop, D. R.; Jimenez, J. L. Interpretation of organic components from Positive Matrix Factorization of aerosol mass spectrometric data. *Atmos. Chem. and Phys.* **2009**. 9(9), 2891–2918.
- (3) Paatero, P., Hopke, P. K., Song, X.-H., & Ramadan, Z.: Understanding and controlling rotations in factor analytic models. Chemometr and Intell Lab Syst, 60(1–2), 253–264. 2002.
- (4) Zhang, Q.; Jimenez, J.; Canagaratna, M.; Ulbrich, I.; Ng, N.; Worsnop, D.; Sun, Y. Understanding atmospheric organic aerosols via factor analysis of aerosol mass spectrometry: a review. *Analy. Bioanaly. Chem.* **2011**. 401(10), 3045–3067.